SP.
WL

BEND RESEARCH, INC.

MASTER

64550 RESEARCH ROAD • BEND, OREGON 97701 • TELEPHONE (503) 382-4100

DISCLAIMER

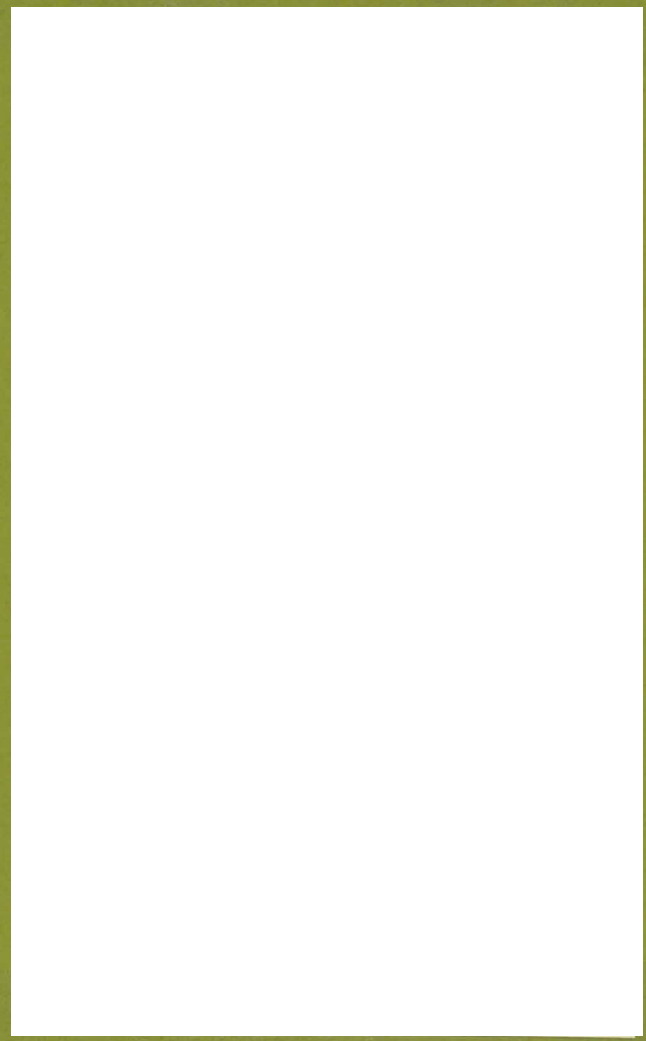

DOE/SALINITY
August 16, 1978

FINAL REPORT

MEMBRANE RESEARCH FOR SALINITY GRADIENT ENERGY PRODUCTION

Contract No. EG-77-C-05-5525

Contributors to this Report:

H.K. Lonsdale (Principal Investigator)
R.W. Baker
K.L. Lee
K.L. Smith

TABLE OF CONTENTS

SUMMARY

This report describes the results of an initial feasibility study of pressure retarded osmosis (PRO) as a power generation technique from various salinity gradient resources. A number of flat sheet reverse osmosis membranes were evaluated. Reverse osmosis (RO) and direct osmosis (DO) experiments were used to predict the performance of the membranes under PRO conditions. Based on this work, we conclude:

1. Concentration polarization is a major problem in PRO. If not controlled, concentration polarization can reduce the water flux through PRO membranes to a fraction of the value expected from RO tests. Two types of concentration polarization exist. The first is external concentration polarization in the liquid boundary layers on either side of the membrane. External concentration polarization can be minimized by stirring the solutions to reduce the thickness of these liquid boundary layers. The second type of concentration polarization is internal concentration polarization which occurs in the porous substructure of anisotopic membranes and is unaffected by stirring. Internal concentration polarization can only be reduced to an acceptable level by using membranes with an open microporous substructure, such as cellulose acetate asymmetric (Loeb-Sourirajan) membranes.

2. Internal concentration polarization cannot be overcome by using brines of highly rejected salts such as magnesium sulfate.

3. Useful PRO membranes do not require the ultrahigh permselectivity necessary in reverse osmosis, and a trade-off between flux and salt rejection is possible. If the salt rejection is too low, however, internal concentration polarization due to excessive salt leakage can limit the flux. PRO membranes should have the combination of high salt rejection in the skin layer and high rates of salt diffusion in the porous support layer to avoid internal concentration polarization. Composite membranes, despite their high water permeabilities and high salt rejections in RO, are not suitable for PRO because of severe internal concentration polarization, even at very modest fluxes. This internal concentration polarization results from the pores of the membrane structure being apparently filled with a crosslinked gel which interferes with salt diffusion in this substructure.

4. Hollow fiber membranes are likely the most promising membrane geometry for two reasons: they allow control of external concentration polarization by circulation of solution on both sides of the membrane, and they are the cheapest form of membrane currently available.

5. The flux through a direct osmosis membrane using concentrated brine as the salt solution and seawater as the dilute solution is approximately half of the flux obtained when fresh water is used on the dilute side of the membrane. The PRO salinity gradient system, NaCl brines/seawater, is therefore not a viable resource. However, brackish water solutions containing up to 1% salt can be used with only a 20% drop in flux.

6. Because the operating pressures of PRO systems are lower than those used in RO, compaction of porous membranes due to hydrostatic pressure gradients is reduced. For these membranes, PRO fluxes can be higher than the RO data would suggest.

7. It appears that PRO is an economically viable power generation technique, provided that asymmetric (Loeb-Sourirajan-type) hollow fibers can be prepared with membrane fluxes comparable to flat sheet membranes.

I. INTRODUCTION

This is the final report on Department of Energy Contract No. EG-77-C-05-5525, entitled "Membrane Research for Salinity Gradient Energy Production". It covers the period August 18, 1977 through July 31, 1978.

A large quantity of potential energy is stored in the waters of the earth, as a result of the unequal concentrations of salt in fresh water and seawater. This energy, in reality a form of solar energy, is now released as low grade heat when fresh waters mix with the sea. The amounts of energy involved are vast. It has been estimated[1] that the energy of mixing of the Columbia River with the Pacific Ocean is equal to the energy now generated by the entire system of dams on the river, i.e., some 4000 electrical megawatts. Much of this energy could be recovered by allowing the waters to mix through an osmotic membrane, thereby converting the osmotic pressure of seawater into a hydrostatic pressure, which could in turn be used to drive a turbine and generate electricity. Such a scheme has been proposed by Loeb[2] and, independently, by Jellinek.[3] The way in which the process would work is illustrated in Figure 1. Loeb has coined the term "pressure retarded osmosis" (PRO) for this process and has already demonstrated its feasibility on a very small scale in Israel.[4] A current summary of the state-of-the-art has been presented by Wick.[5]

In principle, all of the elements of technology required to realize this energy production already exist. The principal element is the semipermeable membrane. High performance membranes of this type have been developed over the past decade and these are now in common use in water desalination by reverse osmosis (RO).[6] It can be readily shown, however, that electricity cannot be generated using current PRO technology at costs competitive with present electrical generation methods. The energy of mixing of fresh water with the sea is 2.8 kw-hr per thousand gallons of fresh water. This is the ideal, or reversible, energy of mixing; not all of this energy could be recovered in a practical system. At current domestic prices, the amount of ideally recoverable energy thus has a value of something less than 10¢ per thousand gallons of fresh water. Because the two processes are so similar, we can assume that the operating costs of pressure retarded osmosis would very likely be comparable to the costs of reverse osmosis. Current costs of desalting seawater by RO are on the order of $2-$4 per thousand gallons of fresh water produced. Thus, an improvement in costs of at least an order of magnitude is required before PRO can be used to produce electricity at competitive prices. And because many of the important

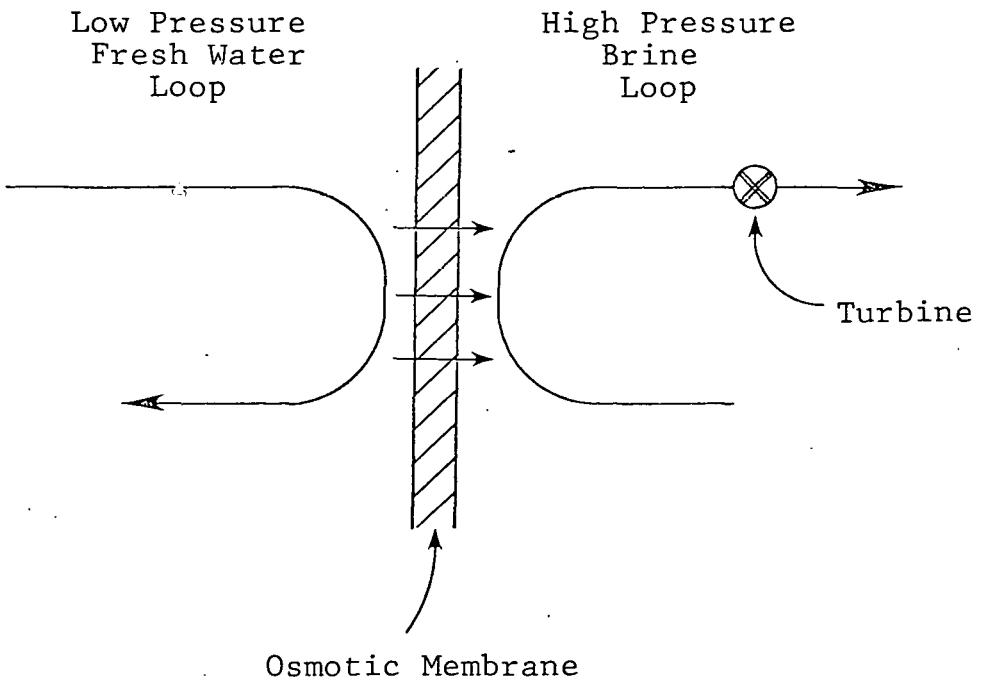

Figure 1. Schematic representation of pressure retarded osmosis. The osmotic pressure of a brine solution is converted to hydrostatic pressure to drive a turbine and generate electricity.

cost elements in the process are rather well fixed (e.g. pumps, turbines, etc.), the improvement required in the economics of the membrane portion of the system will have to be even greater than an order of magnitude.

There are additional ways, of course, in which solar energy could be used in a PRO generator. For example, solar evaporation could be used to produce concentrated brines with even higher osmotic pressures than seawater, which could, in principle, improve the efficiency of the system. It can be readily shown, however, that such improvements will not alter the basic conclusion that improved membrane systems are required.

The principal objective of the present program, therefore, was to examine both existing RO membranes as well as those under development in order to determine whether the required improvements in performance may be achievable. This was thus a feasibility study, aimed at determining the transport properties of membranes and identifying the essential requirements and limitations imposed on osmotic membranes in PRO.

II. THEORY

A. Principles

The relationship between reverse osmosis, pressure retarded osmosis, and direct osmosis is illustrated in Figure 2 for an ideal, perfectly selective semipermeable membrane. In direct osmosis (DO), the semipermeable membrane separates a salt solution on one side of the membrane and water on the other. A flow of water from the water side to the salt solution then takes place due to the difference in osmotic pressures between the two solutions. If the salt side is gradually pressurized, the water flow will decrease until no flow occurs when the applied pressure equals the osmotic pressure of the salt solution. This regime in which there is a flow of water into a pressurized salt solution is known as pressure retarded osmosis. Reverse osmosis occurs when the hydrostatic pressure applied to a salt solution is greater than the osmotic pressure. In this case, there is a flow of water from the salt solution side to the water side of the membrane.

The water flux, J_w, for these ideal membranes can be related to pressure by the simple equation

$$J_w = A(\Delta\pi - \Delta P), \qquad (1)$$

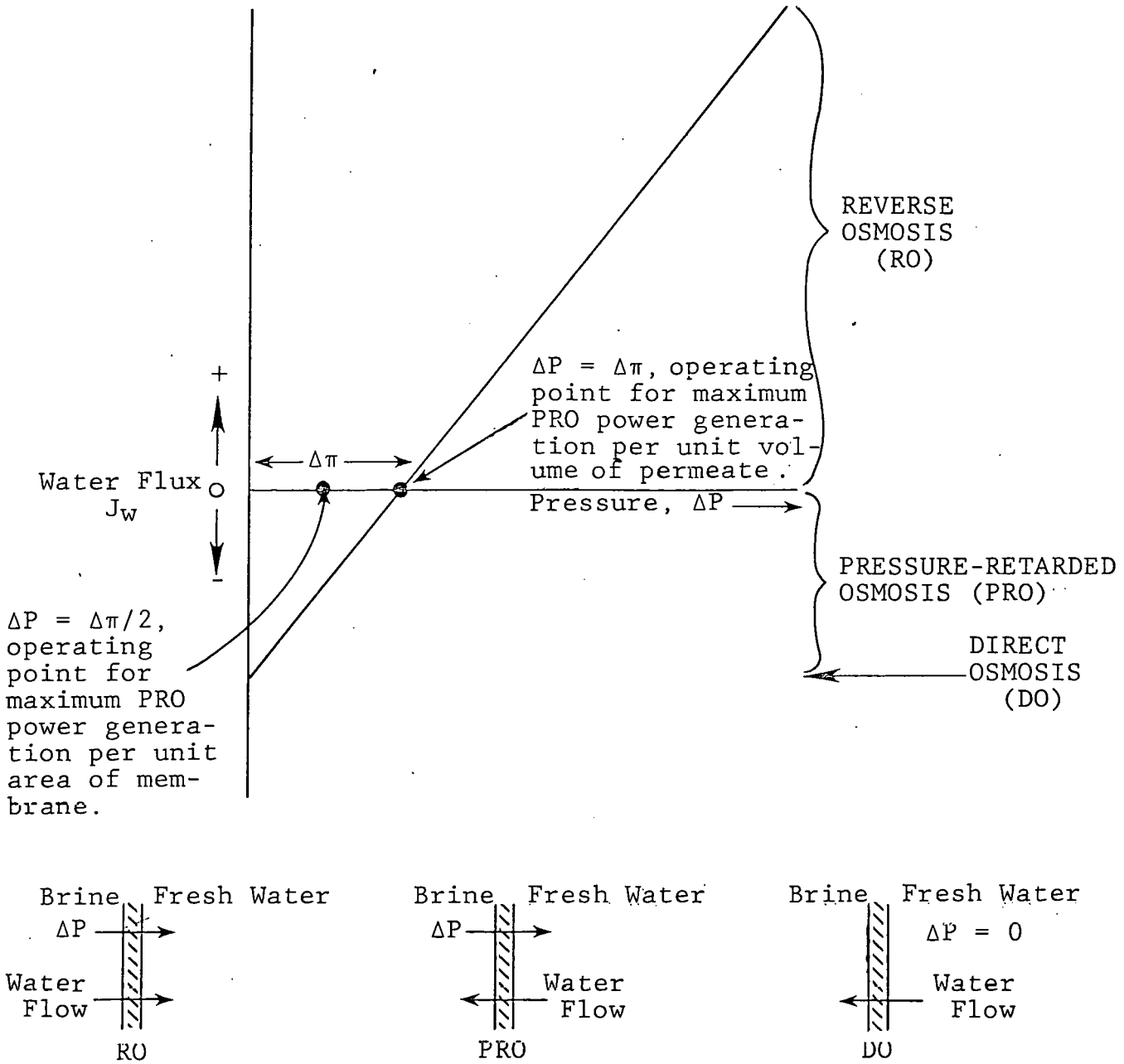

Figure 2. The relationship between reverse osmosis, pressure retarded osmosis, and direct osmosis.

where A is the membrane water permeation constant, $\Delta\pi$ is the osmotic pressure difference across the membrane, and ΔP is the hydrostatic pressure difference across the membrane.

In PRO, the power per unit membrane area that can be generated is equal to the product of the water flux across the membrane and the hydrostatic pressure of the salt solution. The maximum power per unit volume of solution transported by osmosis is therefore obtained at the maximum hydrostatic pressure under which PRO takes place, i.e. the osmotic pressure, π. At this pressure, however, the transmembrane water flux would be negligible, and a very large membrane area would have to be used, resulting in high capital costs for the system. It is preferable, therefore, to operate PRO systems under conditions corresponding to the maximum power per unit membrane area, in order to minimize capital costs. It can be shown that these conditions correspond to a salt side pressure of $\Delta\pi/2$. The water flux in this case, from Equation (1), is $A\Delta\pi/2$. Thus,

$$\text{power/unit membrane area} = \left(\frac{A\Delta\pi}{2}\right)\left(\frac{\Delta\pi}{2}\right) = \frac{A\Delta\pi^2}{4}. \qquad (2)$$

Equation (2) shows that the maximum output of a PRO system increases in direct proportion to the membrane water permeability constant, A, and thus high flux membranes are preferred. The power output is also proportional to the square of the osmotic pressure, or salt concentration, on the salt side of the membrane. That is, doubling the salt concentration, in principle, increases the power generating capacity of a PRO system four fold. The dependence of power on the square of the salt concentration arises because increasing the salt concentration increases both the pressure at which the system operates and the flow rate through the membrane.

B. Concentration Polarization

In practice, real membranes are not perfectly permselective and a small amount of salt permeates the membrane. This salt permeate has two effects. The first is to lower the pressure at which the hydrostatic and osmotic flows are balanced from $\Delta\pi$ to $\Delta\pi_{obs}$. In general, this is not a serious effect unless the membrane has very poor salt-rejecting characteristics. The second effect of salt permeation through the membrane, concentration polarization, is much more serious. Concentration polarization effects can be external or internal. External concentration polarization in direct osmosis is illustrated in Figure 3. In this figure, it is assumed that the membrane is homogeneous, and for simplicity, the salt partition coefficient in the membrane is taken to be unity. As shown

in Figure 3, the concentrations of salt at the membrane interfaces are different from the bulk solution concentrations. This is caused by the flow of salt and water through the membrane in opposite directions, producing a more dilute solution at the salt side membrane interface and a more concentrated solution at the water side interface of the membrane. The actual osmotic driving force across the membrane is then $\pi_2-\pi_4$, corresponding to the salt concentrations, C_2 and C_4, in the so-called boundary layers on each side of the membrane. This driving force is lower than the apparent value, $\pi_1-\pi_5$, corresponding to the bulk solution salt concentrations, C_1 and C_5. This problem can be overcome by stirring the solutions on both sides of the membrane to minimize these boundary layers. With flat sheet membranes, appropriate stirring is easily achieved on the salt side of the membrane. However, on the water side of the membrane, a support layer is required to withstand the hydrostatic pressure across the membrane. This support interferes with good stirring, and prevents elimination of the boundary layer. For this reason, PRO experiments with flat sheet membranes are difficult to perform. It is therefore preferable to extrapolate the performance of the membranes under PRO conditions from the results of DO experiments where the support layer can be dispensed with because there is no hydrostatic pressure difference. For this same reason, practical PRO systems will almost certainly be limited to hollow fiber membranes, which need no support layer to withstand the salt side pressure, and with which good stirring on both sides of the membrane is achieved.

Internal concentration polarization of the membranes caused by salt permeation through the membrane is much more difficult to control. All RO membranes with useful water permeabilities are anisotropic, with a very thin salt-rejecting "skin" layer on one side of the membrane. The remainder of the membrane is a fairly porous matrix that serves as a support for the skin. It is the build-up of salt within this porous support layer that constitutes internal concentration polarization, as shown in Figure 4. As before, there exists some polarization at the outer surfaces of the membrane which can be controlled by stirring. However, stirring does not affect the concentration polarization within the membrane. The osmotic driving force is not then $\pi_2-\pi_4$, corresponding to the concentrations C_2 and C_4, but $\pi_2-\pi_3$, corresponding to the concentrations C_2 and C_3. As will be shown below, this internal concentration polarization can be a very serious problem, reducing the flux in DO and PRO experiments to a fraction of the value predicted from RO experiments. The problem does not occur in RO because the water flux is in the same direction as the salt flux, and thus any salt which permeates the membrane is continuously swept away by water permeating the membrane.

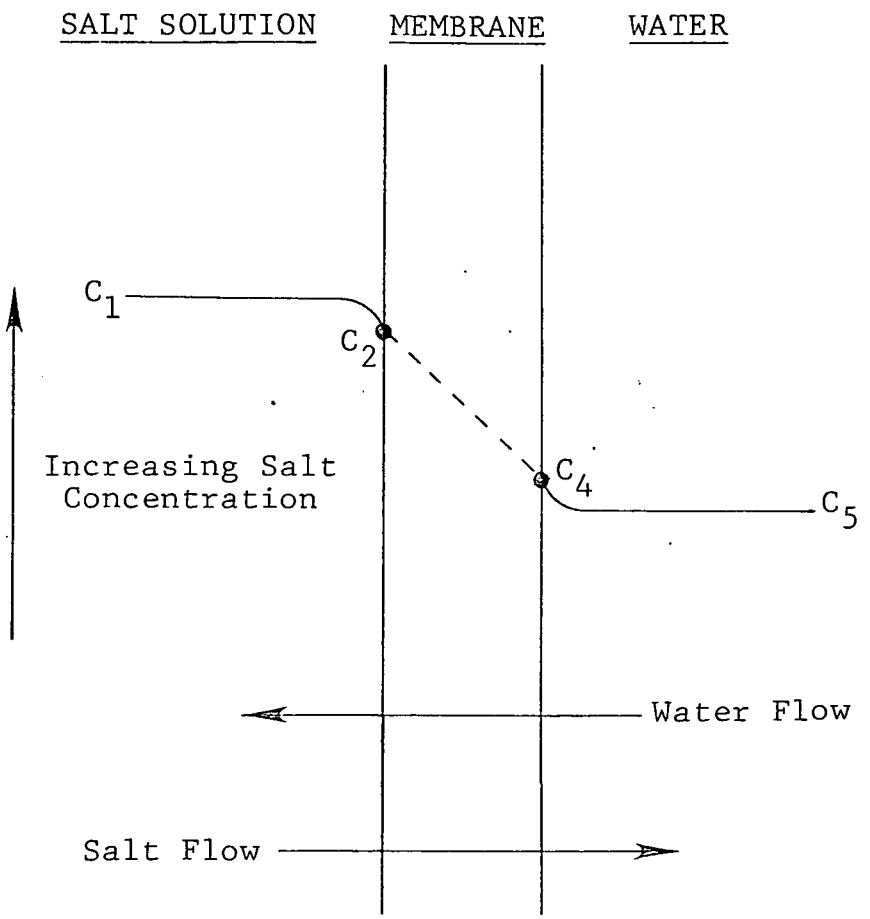

Figure 3. A schematic diagram illustrating external concentration polarization across a homogenous PRO membrane.

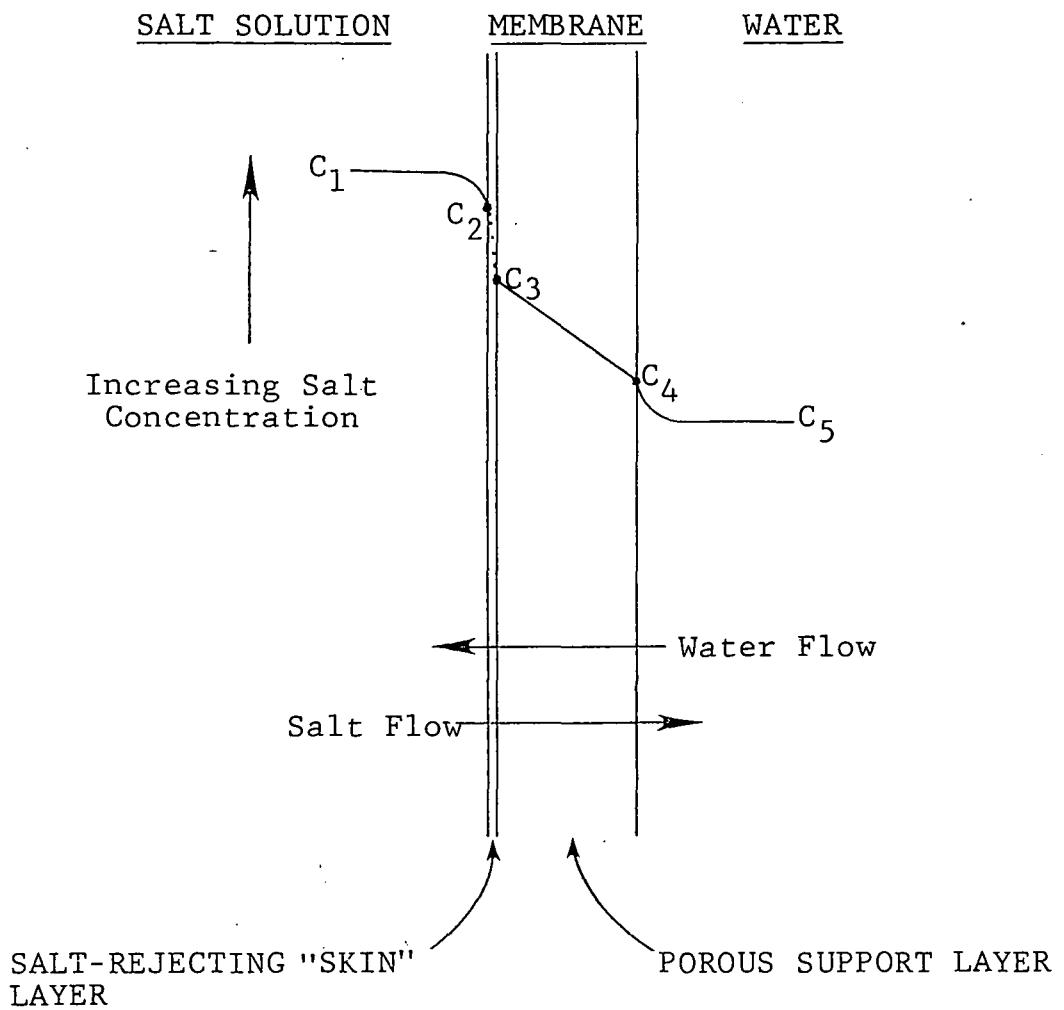

Figure 4. A schematic diagram illustrating internal concentration polarization across an anisotropic PRO membrane.

The actual mathematical treatment of internal concentration polarization in direct osmosis is complex, but sufficiently important to merit attention here. For simplicity, the bulk solutions are assumed to be well stirred, and there is no external concentration polarization. Thus, in Figure 4, $C_2 = C_1$ and $C_4 = C_5$. The water flux across the salt-rejecting skin is then given by Equation (1), with $\Delta P = 0$:

$$J_w = A(\Pi_2 - \Pi_3). \tag{3}$$

The salt transported across the rejecting layer can be written as[7]

$$-J_s = B(C_2 - C_3), \tag{4}$$

where B is the salt permeation constant. The salt flux is negative because the direction of salt flow is opposite to that of the water flow. In the porous layer, the salt flow consists of two components acting in opposite directions: a diffusive part due to diffusion down the salt concentration gradient, and a convective part due to the bulk flow of water through the system. The salt flux is thus written:

$$-J_s = D_s \varepsilon \frac{dC(x)}{dx} - J_w C(x), \tag{5}$$

where ε is the porosity of the substrate and is assumed equal to the volume fraction occupied by capillary water in the membrane. Typically, $\varepsilon > 0.5$. Combining Equations (4) and (5) yields:

$$B(C_2 - C_3) = D_s \varepsilon \frac{dC(x)}{dx} - J_w C(x). \tag{6}$$

The boundary conditions for the direct osmosis case are:

$$C(x) = C_4 \text{ at } x = 0$$

$$C(x) = C_3 \text{ at } x = \tau t,$$

where t is the thickness of the porous substrate, typically 100 μm, and τ is a tortuosity factor. The tortuosity increases the effective thickness of the membrane. Typically, in simple systems, τ is approximately equal to $1/\varepsilon$. With these boundary conditions, Equation (6) can be integrated to give:

One method of characterizing the extent of internal concentration polarization is to define an internal concentration polarization coefficient, Q, equal to the fractional decrease in the membrane flux from the theoretical flux in the absence of polarization. Q is thus defined as

$$Q \equiv \frac{J_{w_o} - J_w}{J_w} , \tag{12}$$

where J_w is the flux in the presence of polarization obtained from Equations (10) or (11), and J_{w_o} is the flux in the absence of polarization ($C_3 = C_4$), obtained from Equation (3). Thus, Q = 0 represents no internal polarization ($J_w = J_{w_o}$), and Q = 1 represents complete polarization ($J_w = 0$). An equivalent definition of Q arises from the salt concentration profile in Figure 4:

$$Q = \frac{C_3 - C_4}{C_2 - C_4} \tag{13}$$

The relationship between the various parameters incorporated in K (the resistance to salt transport through the porous sublayer) and the extent of internal concentration polarization, Q, is illustrated by plotting Q as a function of J_w for different values of K. Figures 5 and 6, differing only in the magnitude of B (a measure of the membrane salt permeability), show this relationship for the simplest case of the brine/pure water system ($C_4 = 0$). The curves are derived from Equation (11), using values for the parameters representative of reverse osmosis membranes.

The most significant features of this family of curves are:

a. Internal concentration polarization increases monotonically with water flux. Physically, this is because the diffusion of salt through the porous sublayer is opposed by the convective osmotic water flow. Salt therefore tends to accumulate at the interface between the rejecting skin and the porous sublayer. Increasing osmotic driving forces at high Q values would bring about progressively smaller gains in water flux. Alternatively, the flux at which Q asymptotically approaches unity defines the maximum water flux attainable with a given salt, regardless of brine content.

In the limit of zero water flux, on the other hand, Q approaches a non-zero lower limit. (In practice, of course, this situation can be realized only if the brine is pressurized, so that $J_w = 0$, even though $\Delta\Pi \neq 0$). Here, the transport of salt is unaffected by convection and therefore proceeds by diffusion alone, driven by the existing concentration gradient in the porous sublayer.

$$\frac{B(C_2 - C_3) + J_w C_3}{B(C_2 - C_3) + J_w C_4} = \exp\ (J_w \tau t / D_s \varepsilon), \qquad (7)$$

which rearranges to:

$$\frac{C_3}{C_2} = \frac{B(e^{J_w K} - 1) + J_w \frac{C_4}{C_2} e^{J_w K}}{B(e^{J_w K} - 1) + J_w}, \qquad (8)$$

where $K = \tau t / D_s \varepsilon$. The values of all membrane parameters on the right-hand side of Equation (8) are either known or can be estimated for a given membrane. Thus, the effective concentration gradient of salt across the skin layer may be computed. In the special case of a brine/pure water system, $C_4 = 0$. Equation (8) therefore reduces to the even simpler form:

$$\frac{C_3}{C_2} = \left[\frac{J_w}{B(e^{J_w K} - 1)} + 1\right]^{-1}. \qquad (9)$$

K, in Equations (8) and (9), is a measure of the resistance of the porous sublayer to salt transport. A high value of K indicates a high resistance to salt transport, due to either a tortuous path in a thick membrane, a low salt diffusion coefficient, or a low porosity. Correspondingly, a low value of K indicates a low resistance to salt passage.

If the ratio of salt concentrations is assumed to be approximately equal to the ratio of osmotic pressures, i.e., $C_i/C_j = \pi_i/\pi_j$, then Equation (3) may be combined with Equations (8) and (9) to yield, respectively,

$$J_w = A\pi_2 \left[1 - \frac{C_4}{C_2} e^{J_w K}\right] - B\left[e^{J_w K} - 1\right]; \quad C_2 > C_4 > 0, \qquad (10)$$

and

$$J_w = A\pi_2 - B\left[e^{J_w K} - 1\right]; \quad C_4 = 0. \qquad (11)$$

Equations (10) and (11) relate the direct osmosis water flux to the characteristics of the membrane and to the osmotic pressure of the brine. Equation (11) may be solved numerically for J_w using π_2 values derived from appropriate osmotic coefficients.(8)

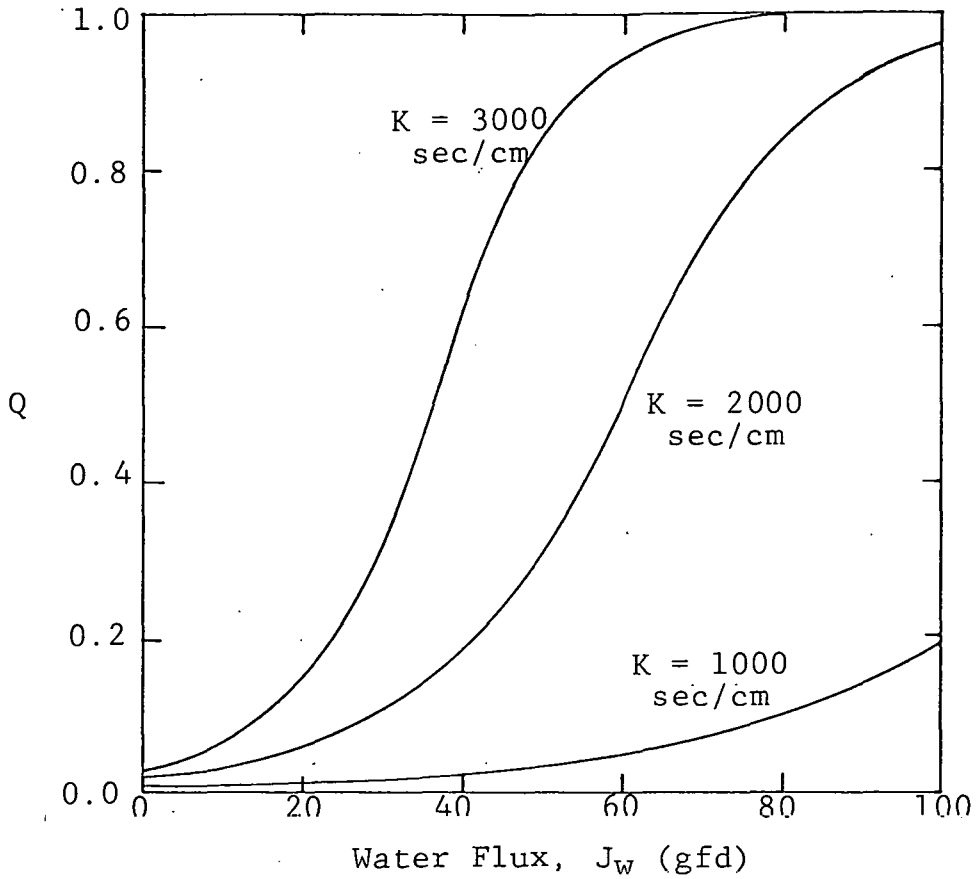

Figure 5. Effect of the direct osmosis water flux, J_w, on the internal concentration polarization parameter, Q, for different values of K. B = 10^{-5} cm/sec.

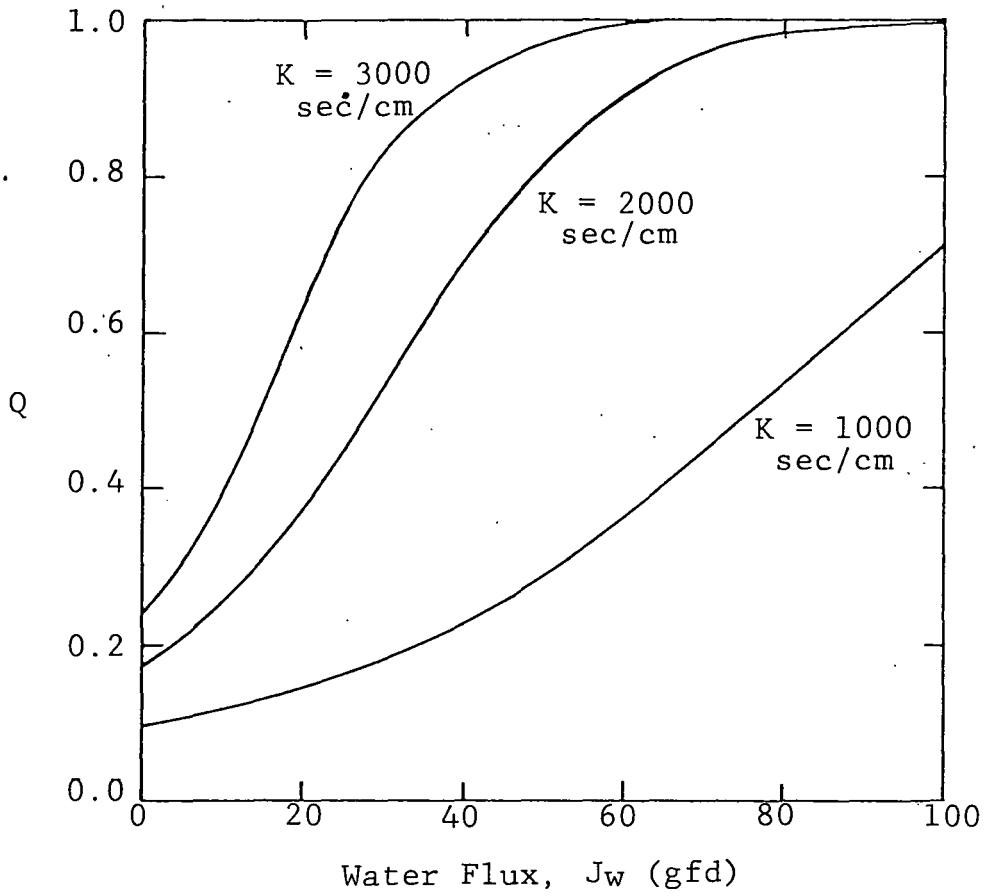

Figure 6. Effect of the direct osmosis water flux, J_w, on the internal concentration polarization parameter, Q, for different values of K. B = 10^{-4} cm/sec.

b. Internal concentration polarization is increased by increasing the membrane thickness or tortuosity, or by decreasing the diffusion coefficient of the salt or porosity of the porous sublayer. Thinner membranes will therefore exhibit less concentration polarization, all other factors being equal.

c. Poor salt rejection properties of the skin region of the membrane, manifested in a high salt permeation constant, B, lead to a high degree of concentration polarization.

Figure 7 shows the concentration polarization curves for the case when the dilute side of the membrane contains increasing quantities of salt. Internal concentration polarization is much worse in this case, since the convective flux of water carries salt into the porous sublayer of the membrane. Thus, as the concentration of salt on the porous side of the membrane increases, the extent of internal concentration polarization also increases, at a given osmotic water flow.

The approach to Q = 1 of the curves shown in Figure 7 with C_4/C_2 greater than zero is clearly non-asymptotic. This may be explained conceptually by the mechanism for the dissipation of salt from the porous sublayer. In a brine/water system, only pure water flows into the porous sublayer. There is always a finite difference in salt concentration between the underside of the rejecting skin and the external side of the porous sublayer (pure water). Consequently, there is a continuous diffusive dissipation of the salt, and C_3 is always less than C_2. The approach of the Q vs. J_w curve to Q = 1 is therefore asymptotic under these boundary conditions. By contrast, the osmotic water flow in a brine/brine system carries with it a certain amount of salt into the porous sublayer. When the sum of this convective salt flow plus the "leakage" across the rejecting skin exceeds the rate at which salt can diffuse out of the porous sublayer, C_3 increases until it reaches the level of C_2. When this complete polarization (from Equation (13), Q = 1) occurs, the osmotic process stops. There is a well-defined water flux at which the influx of salt exactly balances the dissipation, to cause $C_3 = C_2$. This flux is defined by Equation (8). It can readily be shown that the flux is finite for $C_4/C_2 > 0$, thus explaining the non-asymptotic nature of the curves in Figure 7.

C. Other Factors Affecting PRO Fluxes

Although internal concentration polarization is the dominant factor affecting membrane flux in PRO and DO, two other factors are also significant. The first is "osmotic

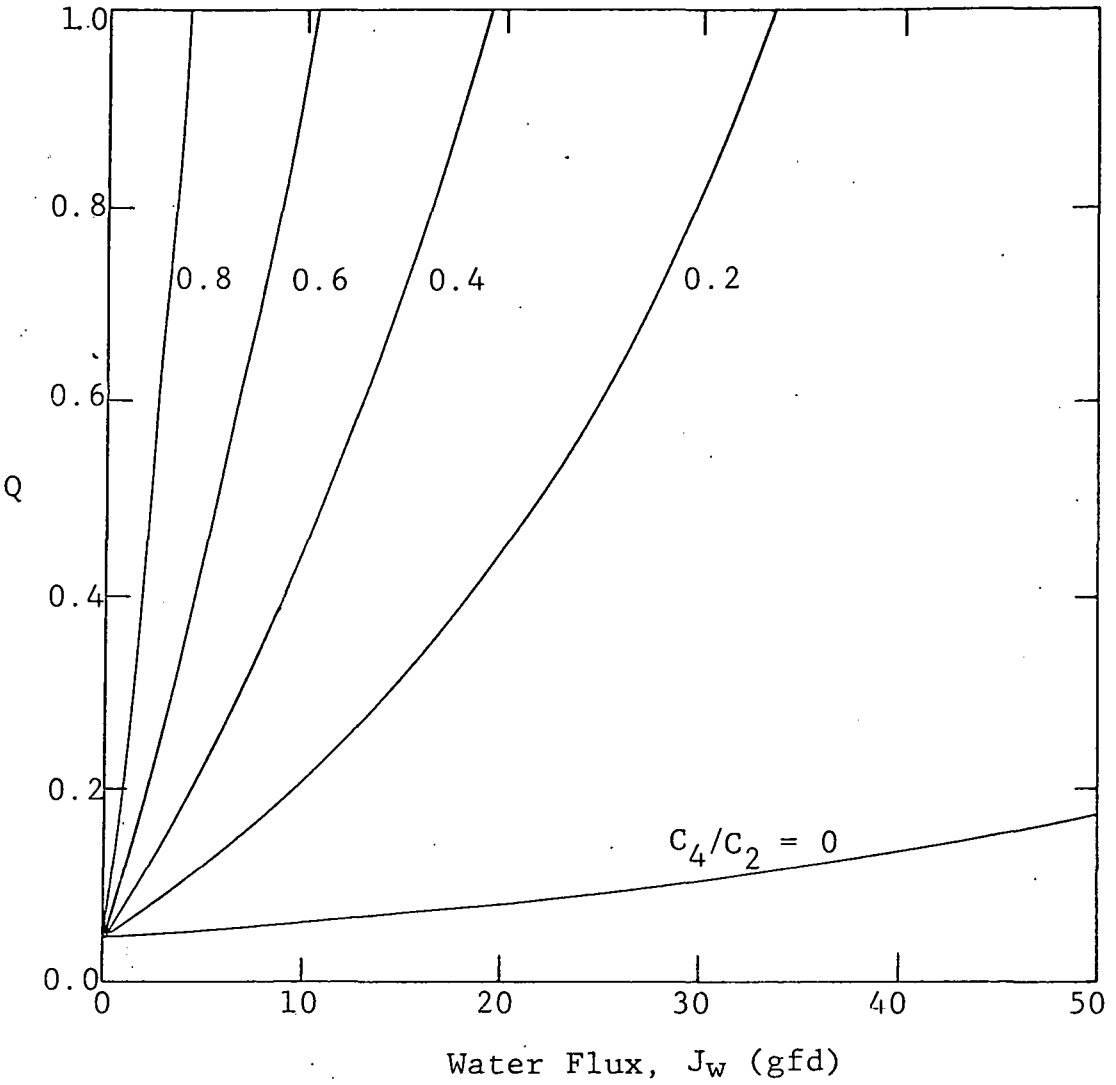

Figure 7. Effects of concentration ratio in a brine/brine system on the extent of internal concentration polarization. $B = 5 \times 10^{-5}$ cm/sec, $K = 1000$ sec/cm.

deswelling", a term used to describe the partial loss of dissolved and capillary water from a membrane contacted with very concentrated salt solutions. This loss of water can lead to a partial collapse of the membrane structure, and consequent lower water and salt permeabilities through the membrane[9]. The actual osmotic flows generated by highly concentrated salt solutions may therefore be less than those predicted by extrapolation of the experimental results with more dilute solutions.

The second factor known to affect membrane flux with these membranes is compaction. When high hydrostatic pressures are applied to the membrane, compaction occurs and lowers the water and salt permeabilities through the membrane. Compaction is particularly noticeable with high-flux, low-salt-rejecting membranes, which usually have a less dense structure than low-flux, high-salt-rejecting membranes. Because of compaction, the water fluxes predicted from RO experiments obtained under hydrostatic pressure gradients may be lower than those obtained in DO under no hydrostatic pressure gradient (that is, $\Delta P = 0$).

D. Potential Salinity Gradient Resources

The first criterion for a useful salinity gradient power generation process is the close proximity of seawater or a brine solution to a supply of fresh or brackish water. However, several types of salt solutions may be used, ranging from different concentrations of NaCl to entirely different salts. The choice of salt affects the composition of the brine system as well as the economics of the process. In our program, several of the possible schemes of practical utility have been investigated. They may be grouped into the following categories:

1. Seawater/Water. This scheme is exemplified by a river terminating at the sea. In principle, a PRO plant could be constructed at every estuary; thus, the size of the potential resource is enormous. However, it is a relatively low-grade resource, since the osmotic pressure of seawater is only 24 atmospheres. This type of PRO plant would therefore operate at a seawater pressure of 10-12 atmospheres ($\Delta\pi/2$), and the osmotic pressure gradient available to drive water through the membrane would also be 10-12 atmospheres. Membrane fluxes under this presure gradient would be small, and the capital costs of the membrane required to generate useful quantities of electricity would be correspondingly high.

2. Brines/Water. The osmotic pressure of NaCl brines can reach 350 atmospheres. Thus, as shown in Equation (2), the power produced using these solutions could in principle be much higher than with seawater, even if the membranes suffer partial osmotic deswelling at the high brine concentrations. On the other hand, although this is a much higher-grade resource, the potential quantity of energy extractable is much smaller, since concentrated brines are generally only found in deserts where the available fresh water is both limited and valuable. Wick and Isaacs[10] have recently suggested using salt domes as a brine source, in which case the plants could be located closer to available fresh water sources. However, the diluted brine effluent would then pose a significant disposal problem.

3. Brines/Seawater, Brines/Brackish Water. One possible method of increasing the utility of brine lakes as a salinity gradient resource is to use seawater or brackish water on the dilute side of the membrane. There are several locations in the southern and southwestern United States where this would be feasible. The diluted brine would be recycled to the brine lake to be reconstituted by solar evaporation. This is an attractive approach if the internal concentration polarization effects described earlier can be controlled.

4. Salt Substitutes/Water. A key problem with PRO membranes is leakage of salt across the membrane, leading to internal concentration polarization. This is particularly serious with high-flux, low-salt-rejecting membranes. Highly rejected brines of salt substitutes, such as magnesium sulfate or strong polyelectrolytes (e.g., sodium polystyrene sulfonate), are a possible solution to the problem. Because of their expense, these brines would have to be recovered by solar evaporation after use. Thus, this resource is again limited to desert locations of abundant sunshine but where fresh water supplies are limited.

III. EXPERIMENTAL

A. Membranes

The following flat sheet membranes were selected for testing:

1. Cellulose Acetates. Asymmetric membranes were prepared at the Max-Planck Institute for Biophysics in Frankfurt, Germany, from Bayer Cellit K700 39.1% acetyl cellulose acetate polymer, following a solution-casting procedure first described by Manjikian, et al.[11] Batches of the membrane were annealed at 50°, 60°, 70°, and 80°C, and are designated CA50, CA60, CA70 and CA80, respectively.

2. Polyamide. An asymmetric polyamide membrane, designated BM-05, was obtained from Berghof GmbH.[12]

3. Polybenzimidazolone (PBIL). PBIL is a newly developed reverse osmosis membrane from Teijin Corp. of Japan and Abcor Inc. of Wilmington, Massachusetts.[13,14] An asymmetric membrane of the PBIL polymer was cast onto a polypropylene support by the usual phase inversion technique to give high desalination performance and exceptional chemical stability. Development samples were obtained from Abcor.

4. Composite Membranes. These membranes consist of a salt-rejecting layer deposited on a porous sublayer. The sole function of the sublayer is to provide mechanical support for the ultrathin salt-rejecting layer. Membranes of this type can have salt rejections in excess of 99%.

a. PA-300. This is a polyamide thin-film composite membrane obtained from Universal Oil Products. The salt-rejecting barrier layer is formed by interfacial polymerization of an epichlorohydrin-ethylenediamine condensate, crosslinked by isophthaloyl chloride. This layer is supported on a finely porous polysulfone substrate which accounts for virtually the entire thickness of the composite membrane.[15]

b. NS-101. This membrane was obtained from the North Star Division of Midwest Research Institute. The salt rejecting layer consists of a polyurea formed by the interfacial polymerization of polyethylenimine with isophthaloyl chloride. The support is microporous polysulfone.[16]

c. NS-200. This is a recently developed membrane also obtained from North Star. The active layer of NS-200 is a crosslinked film of polymerized furfuryl alcohol, and the support is again microporous polysulfone.[17]

d. BM-1-C. Berghof GmbH of Tübingen, West Germany supplied this proprietary composite membrane. The only feature known to be in common with other composite membranes is its polysulfone substructure.

We were unable to obtain samples of other types of membranes, including composite membranes prepared by plasma polymerization (Research Triangle Institute, North Carolina), and porous glass membranes (JENAer Glaswerk Schott & Gen., Mainz, West Germany).

B. Reverse Osmosis Test System

A stainless steel reverse osmosis loop, shown schematically in Figure 8, was used for the RO tests.

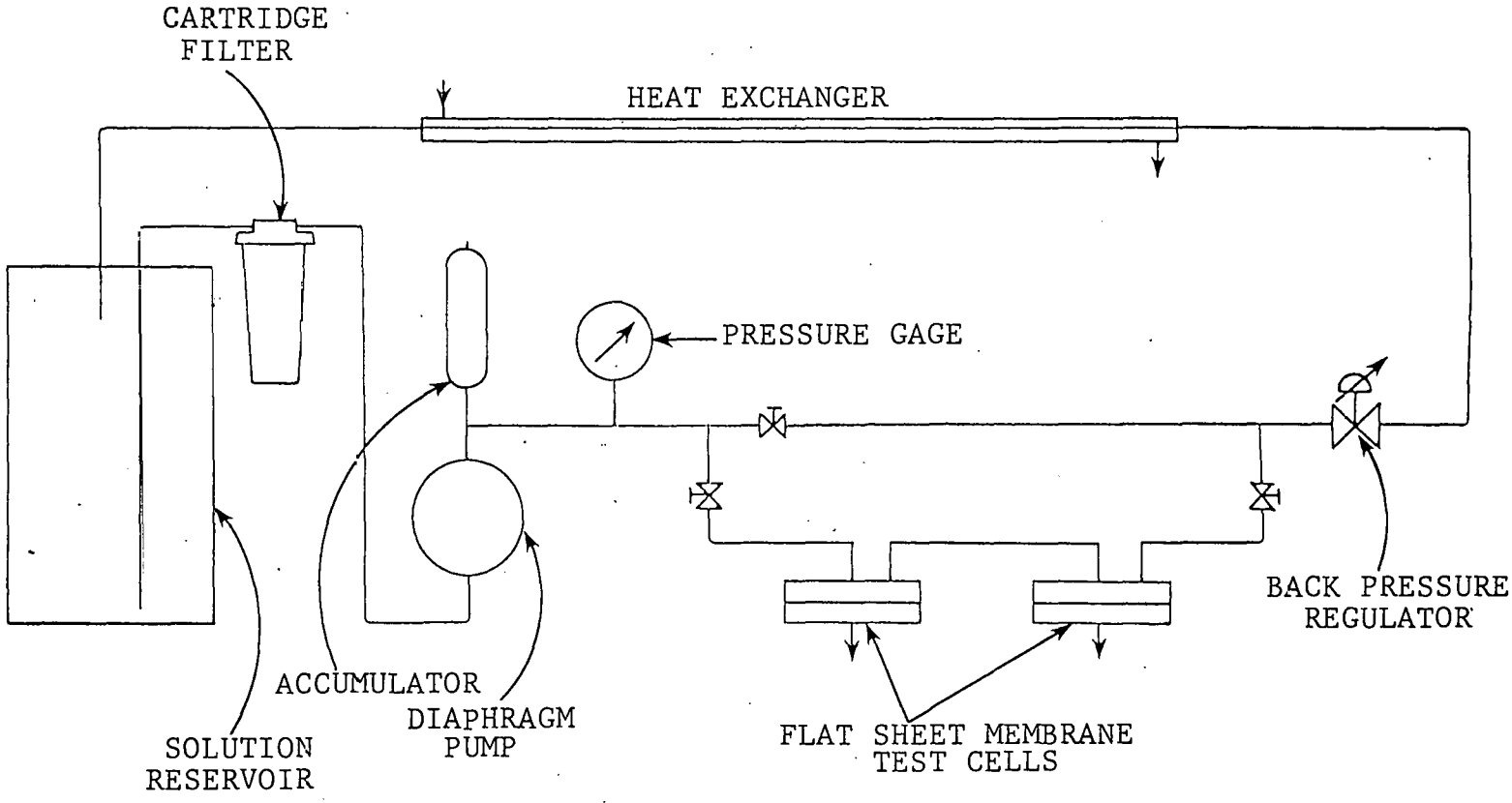

Figure 8. Schematic diagram of reverse osmosis test loop.

Two salts were used for brine make-up: a 3.5% w/v sodium chloride solution was used to simulate seawater, and a 1% w/v magnesium sulfate solution was employed as an alternative osmotic agent to sodium chloride. A high brine recirculation rate across the surface of the membrane was maintained to eliminate concentration polarization. All tests were conducted at 25 $\pm$ 2°C.

In a typical reverse osmosis test, a brine pressure of up to 1200 psig was used. The water and salt fluxes were measured after steady state was reached, typically after about 12 hours. The water flux was then measured as a function of pressure, from 200 to 1200 psig.

C. Direct Osmosis Test System

A glass permeation cell was designed and constructed in which the osmotic water flux and salt flux could be measured concurrently with high precision. A schematic diagram of the cell is shown in Figure 9.

The test membrane was held between the ground glass flanges of the half-cells by a clamp. The enclosed lower half-cell contained the brine. The inlet and outlet on the upper half-cell were connected through a recirculation pump to an external 0.5 or 1.0 liter reservoir of the dilute solution (either water or the weaker brine). An air damper on the pump outlet minimized pulsation in the water circuit, while a stainless steel perforated support screen below the test membrane prevented residual fluctuations in the hydrostatic head from affecting the volume of the brine. Stirring of the liquids on either side of the membrane was provided by a motor-driven glass impeller on the dilute side and a magnetic stirring bar on the brine side. The rate of osmotic flow of water into the brine was measured volumetrically with a pipet. The permeation of salt into the water chamber was determined periodically by measuring the salt concentration of the water with a conductivity bridge. In cases where the water flow into the brine compartment was sufficiently rapid to dilute the brine significantly during an experiment, the brine concentration was also measured at the time the water flux reading was taken.

Two typical direct osmosis runs are shown in Figure 10. The time required before a steady-state flux was reached differed significantly for different membranes. In general, the membranes prepared by the Loeb-Sourirajan technique, such as the BM-05, PBIL, and the cellulose acetate membranes, all reached a steady-state flux within 20 to 50 minutes. However, the composite membranes, such as the PA-300, NS-101, and NS-200, frequently required as long as 100 to 250 minutes.

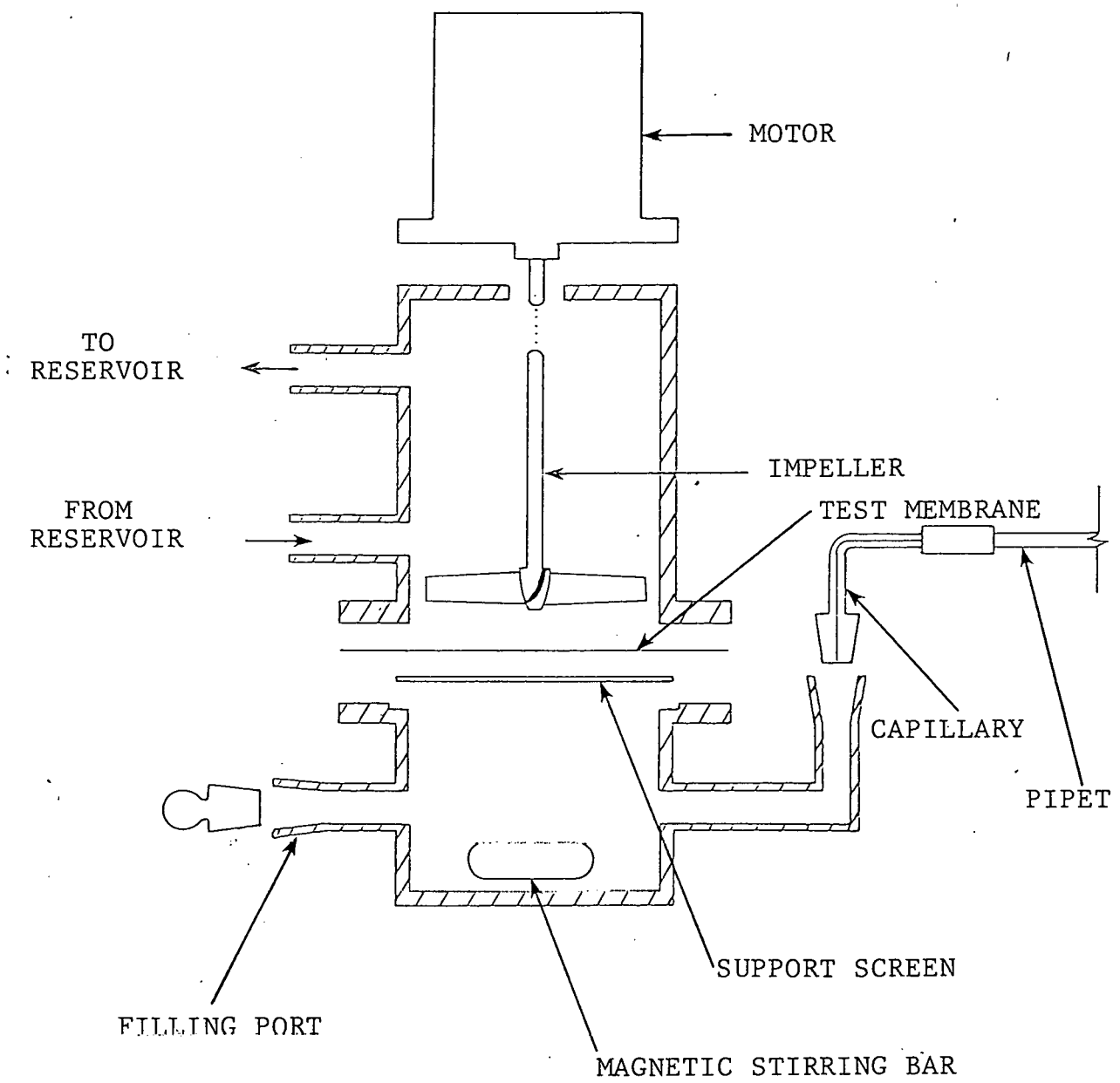

Figure 9. Direct osmosis test cell, exploded view.

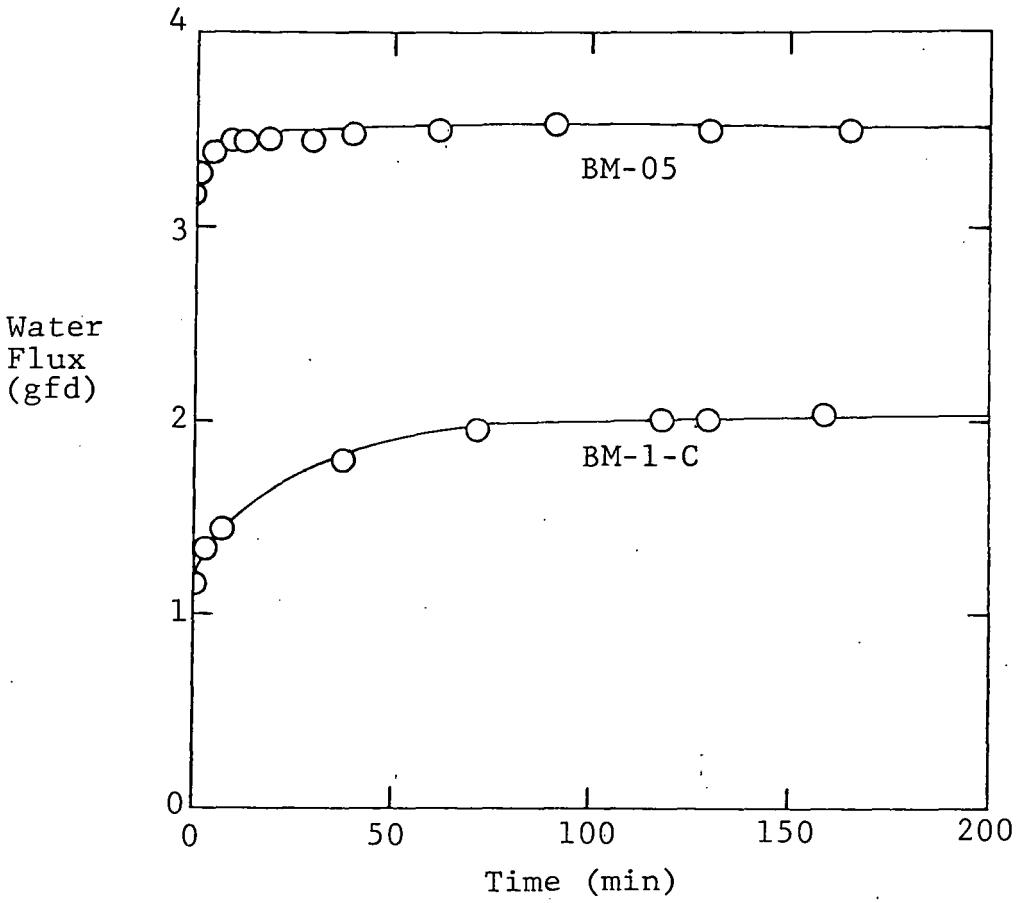

Figure 10. Comparison of an asymmetric membrane (BM-05) and a composite membrane (BM-1-C), showing the different lengths of time elapsed from the beginning of a DO experiment until steady state water fluxes are observed.

The effects of external concentration polarization lower the effective osmotic pressure driving force across the membrane, and are illustrated in Figure 11. When the stirring on the fresh water side of the membrane was stopped, the water flux decreased markedly. This is the result of a higher salt concentration at the porous layer-solution interface than in the bulk solution. Creating a stagnant condition on the brine side produced an additional large flux decline. This decline is expected from the dilution of the brine concentration at that interface by the permeating water. Restarting the water side stirring resulted in partial restoration of the original flux, as the salt build-up at that solution-membrane interface was eliminated. Resumption of stirring in the brine compartment led to a sharp rise of water flux, surpassing the steady state value at the beginning of the experiment. This surge was real and reflected the condition in which the entire salinity gradient was instantaneously imposed across the salt-rejecting layer before the salt concentration profile could again develop within the porous sublayer.

IV. RESULTS AND DISCUSSION

The goal of this program was to evaluate the feasibility of current reverse osmosis membranes in osmotic power generation, using a variety of potential salinity gradient resources. The bulk of our effort centered around sodium chloride brines and synthetic seawater, because these represent by far the largest resource. However, magnesium sulfate and sodium polystyrene sulfonate were also studied as alternate brines. The general approach was first to characterize the membranes by reverse osmosis, which gives the potential membrane performance in the absence of internal concentration polarization and osmotic deswelling. These results were then compared with the results of direct osmosis experiments to determine the importance of internal concentration polarization, osmotic deswelling, and compaction.

A. Salinity Gradient Systems: Seawater/Water, NaCl Brines/Water

1. Reverse Osmosis Experiments. The reverse osmosis flux and rejection characteristics of all the membranes tested are shown in Table 1. An example of a typical flux vs. pressure curve used to generate this data is shown in Figure 12. From the extrapolation of the flux curve to the pressure axis, the observed osmotic pressure, $\Delta\pi_{obs}$, was obtained. This, together with the water permeation constant, was used to calculate the theoretical work available for each membrane, following Equation (2).

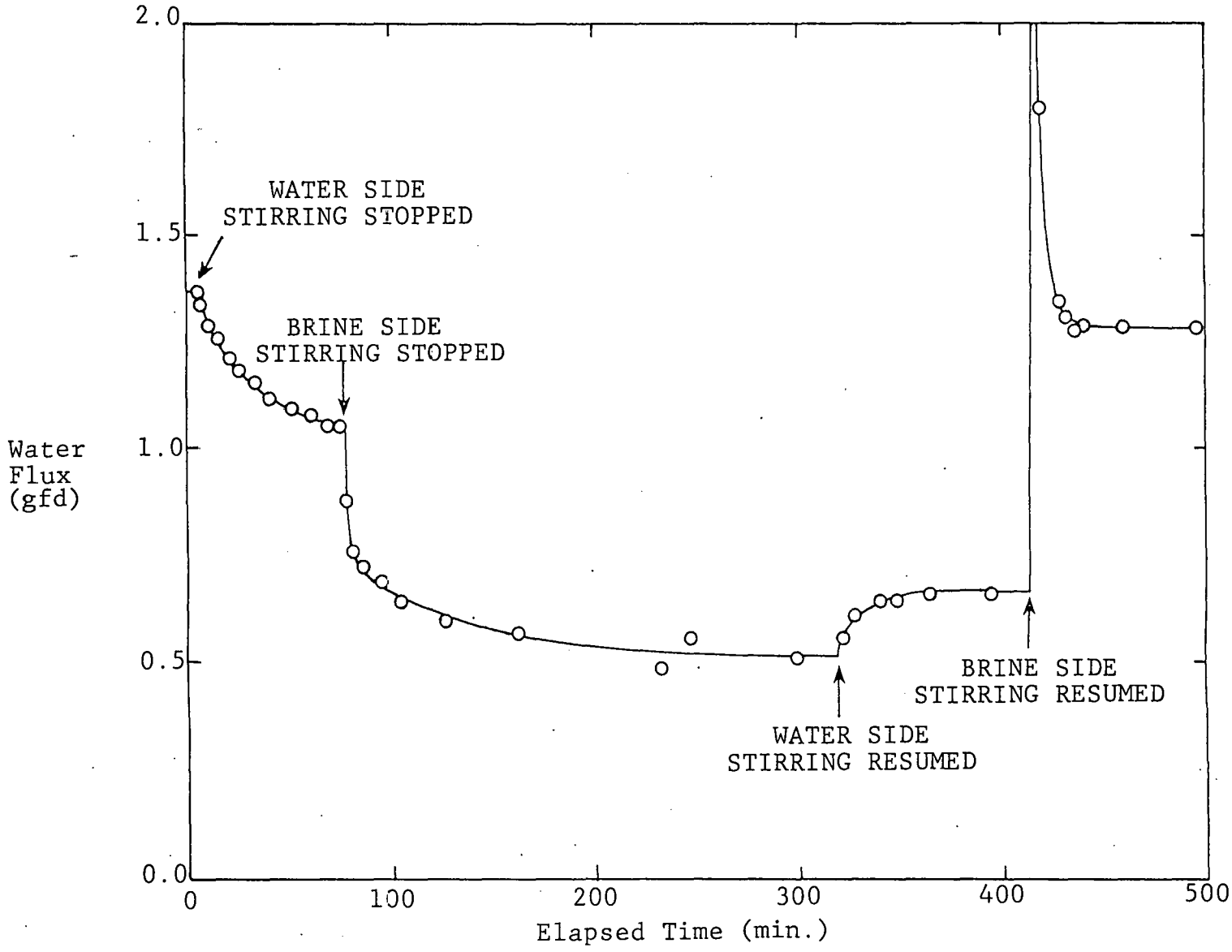

Figure 11. Effects of stirring on either side of a PA-300 membrane on the direct osmosis water flux.

TABLE 1. Transport properties of several RO membranes and their projected direct osmosis performance with 3.5% w/v sodium chloride, $\Delta\pi$ = 28.1 atm.

Membrane	Membrane Thickness (cm)	Water Permeation Constant, A ($\frac{cm^3}{cm^2\text{-sec-atm}}$)	Salt Rejection (%)	Salt Permeation Constant, B (cm/sec)	Observed Osmotic Pressure $\Delta\pi_{obs}$ (atm)	Theoretical Maximum Direct Osmosis Water Flux ($\frac{cm^3}{cm^2\text{-sec}}$)	Theoretical Maximum Direct Osmosis Water Flux (gfd)	Theoretical Maximum Available Work (watt/ft^2)
Cellulose Acetates								
CA80	9.7×10^{-3}	1.0×10^{-5}	87	2.0×10^{-4}	25.5	2.5×10^{-4}	5.3	0.15
CA70	9.4×10^{-3}	3.3×10^{-5}	39	8.7×10^{-3}	15.0	4.7×10^{-4}	9.9	0.17
CA60	1.0×10^{-2}	4.5×10^{-5}	15	3.7×10^{-2}	10.2	4.5×10^{-4}	9.4	0.11
Polyamide								
BM-05	1.1×10^{-2}	4.0×10^{-6}	90	2.3×10^{-5}	27.2	1.7×10^{-4}	2.4	0.07
Polybenzimi-dazolone								
PBIL	2.4×10^{-2}	6.5×10^{-6}	92	3.2×10^{-5}	24.5	1.6×10^{-4}	3.4	0.09
Composites								
FA-300	2.0×10^{-2}	1.1×10^{-5}	99	1.7×10^{-5}	25.1	3.1×10^{-4}	6.5	0.17
NS-101	4.3×10^{-3}	1.2×10^{-5}	94	4.4×10^{-5}	24.6	2.8×10^{-4}	5.9	0.16
NS-200	4.1×10^{-3}	1.0×10^{-5}	94	3.5×10^{-5}	27.2	2.8×10^{-4}	5.9	0.18
BM-1-C	1.2×10^{-2}	8.2×10^{-6}	89	6.1×10^{-5}	20.5	1.7×10^{-4}	3.5	0.08

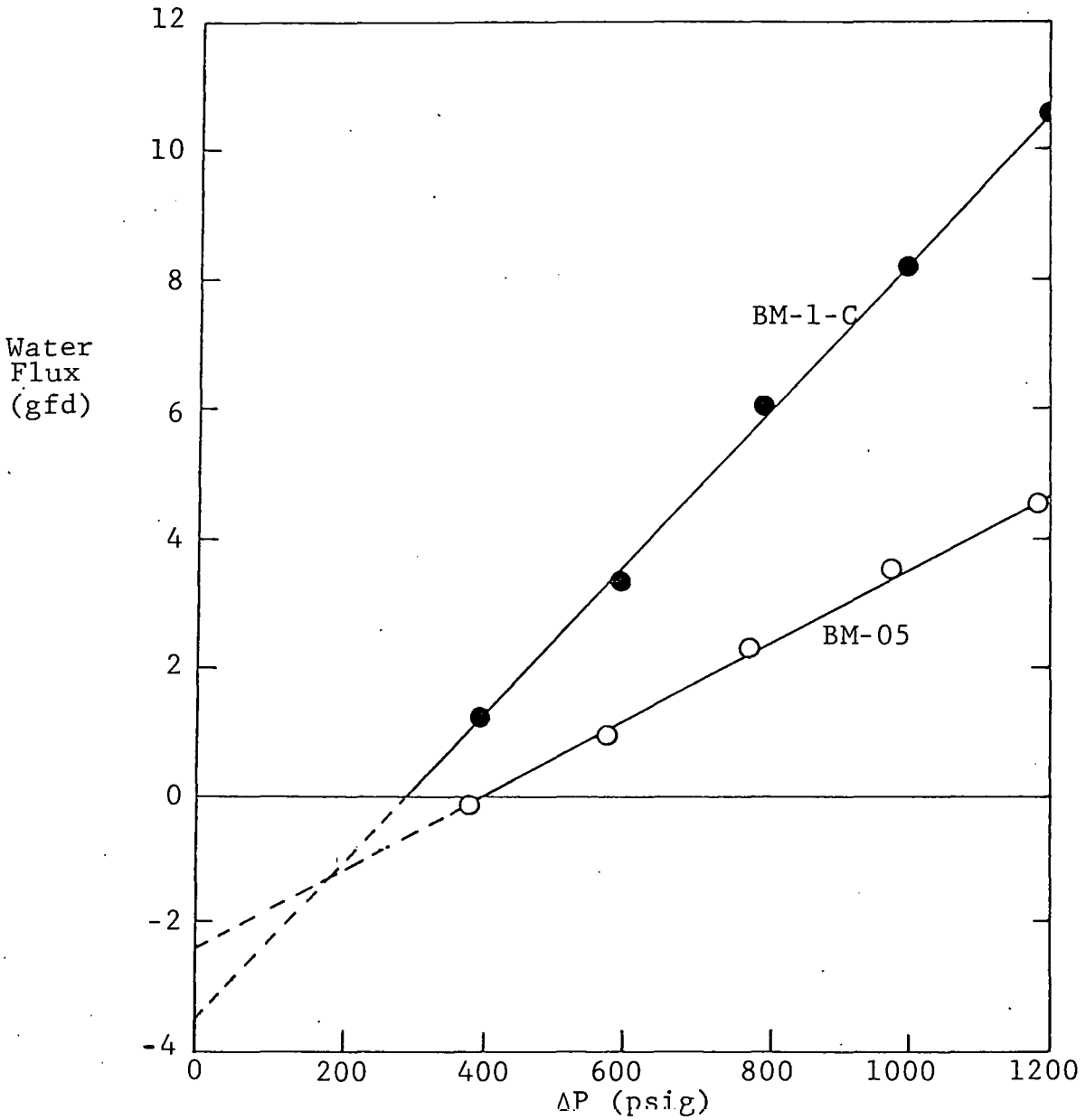

Figure 12. Typical results of a reverse osmosis experiment showing the extrapolation of data to determine the theoretical direct osmosis water flux.

Most of the membranes had high rejections to salt, and thus the observed osmotic pressure was close to the theoretical value. For these membranes, the theoretical work obtainable was approximately proportional to their water permeability. The cellulose acetate membranes represent an interesting series because the permselectivity of these membranes can be easily adjusted by varying the annealing temperature. Higher annealing temperatures result in higher-rejection, lower-flux membranes. With these membranes, it is therefore possible to vary both the observed osmotic pressure and the membrane this flux, the product of which is the potential power per unit membrane area. Experimental results showing the relationship of the annealing temperature to this potential power are presented in Figure 13. It appears that the optimum annealing temperature is approximately 70°C, corresponding to a membrane with a surprisingly low salt rejection of only 39%. However, this inference does not take into account the effects of internal concentration polarization, which, as will be seen later, bias the optimum annealing temperature to higher-salt-rejecting membranes.

2. Direct Osmosis Experiments. The results of direct osmosis tests using sodium chloride solutions are shown in Figures 14 and 15 for asymmetric and composite membranes, respectively. Using the osmotic pressure vs. concentration data shown in the Appendix, it is apparent that the direct osmosis water flux of the majority of the membranes is only a fraction of the value expected from Equation (1) or the reverse osmosis data. Table 2 lists the direct osmosis flux compared to the extrapolated values obtained from reverse osmosis data. The membranes are grouped into three categories.

The first category consists of the composite membranes, where observed fluxes range from 10 to 29% of the expected values. These low fluxes are believed to be due to internal concentration polarization caused by slow salt diffusion in the substructure of the membrane. Composite membranes are made by filling a microporous polysulfone support with a reactive monomer or prepolymer and then initiating a polymerization reaction at the surface of the membrane. The result is a thin, dense, extremely salt-rejecting skin formed on top of a lightly crosslinked gel which partially fills the porous substructure. In reverse osmosis, the gel layer does not interfere with the passage of salt, which is swept out of the porous membrane layer by the permeating water. In PRO and DO, however, this gel prevents rapid diffusive dissipation of salt that has permeated the membrane skin. The osmotic pressure gradient across the skin is therefore reduced to a fraction of its original value. Based on the

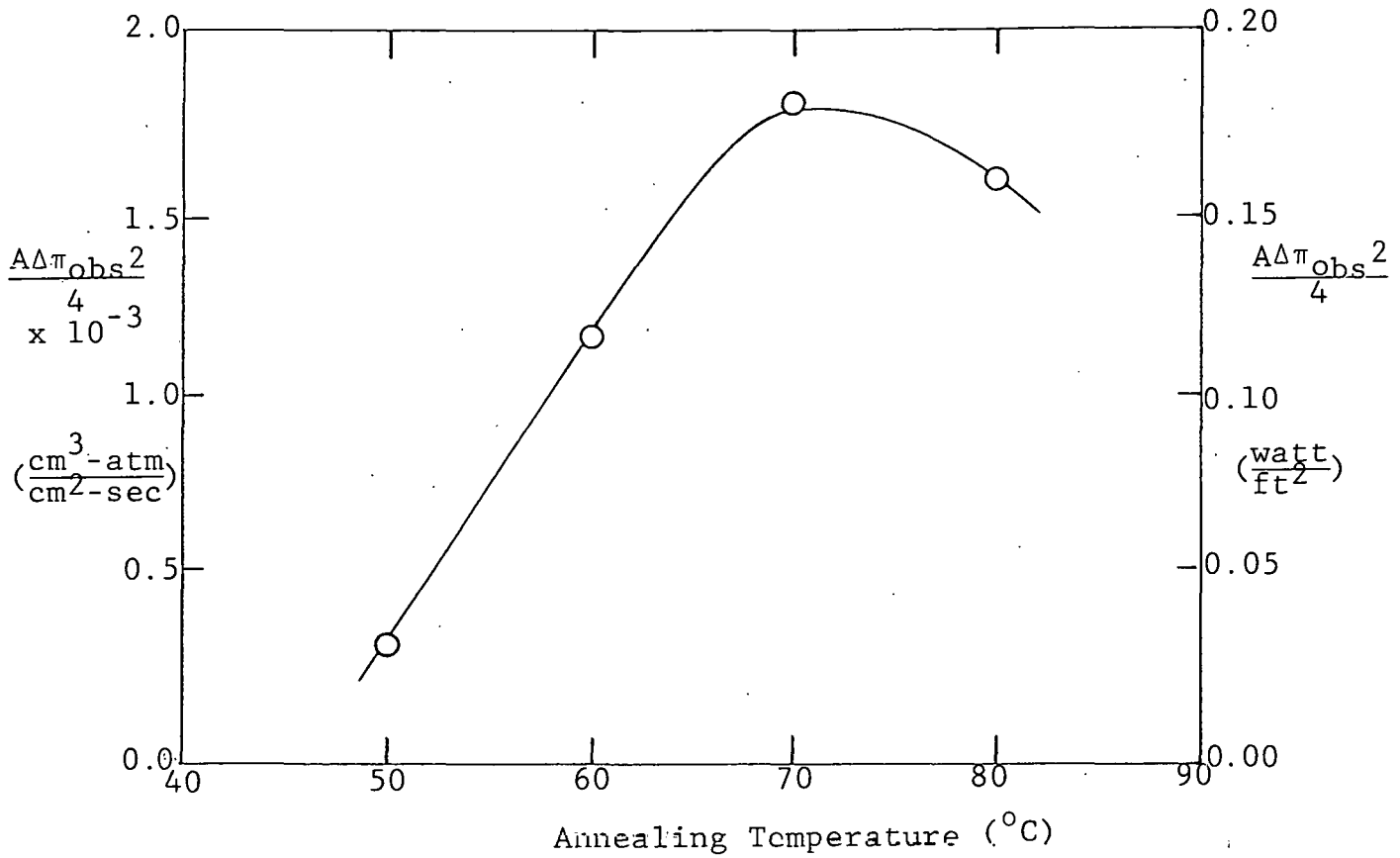

Figure 13. Effect of annealing temperature on the theoretical available work from asymmetric cellulose acetate membranes with 3.5% w/v sodium chloride solutions.

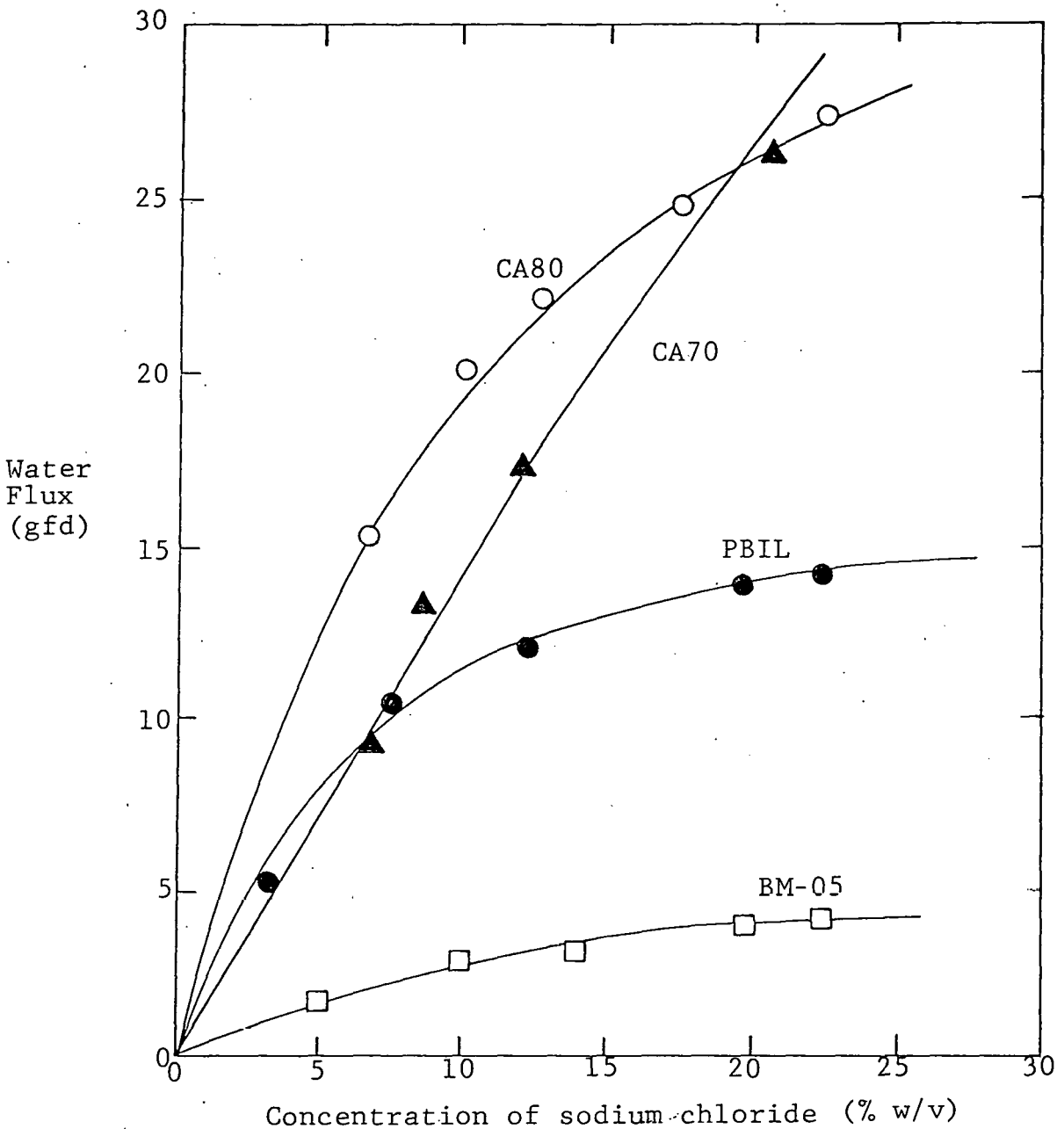

Figure 14. Effect of sodium chloride concentration on direct osmosis water flux across asymmetric membranes.

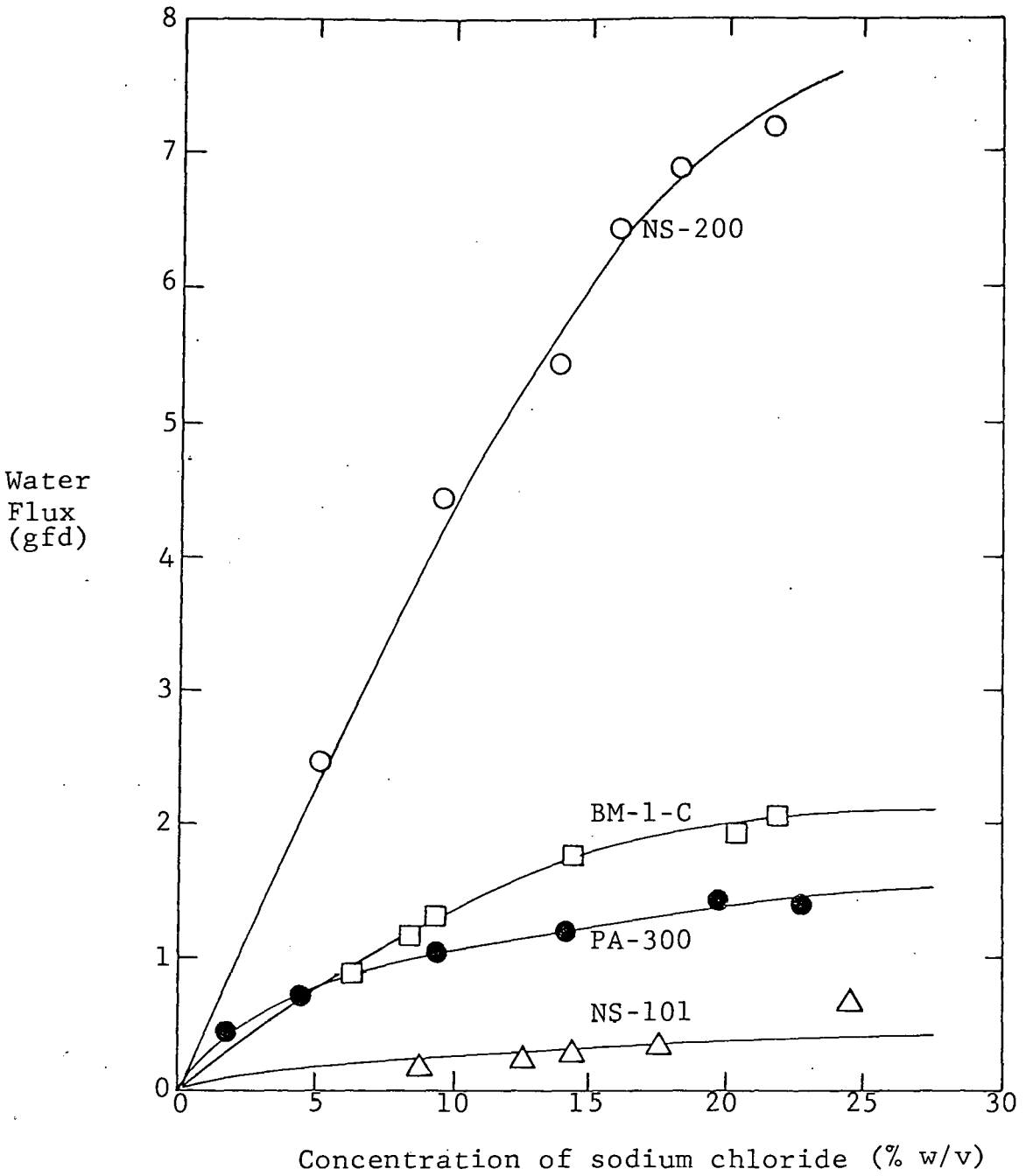

Figure 15. Effects of sodium chloride concentration on direct osmosis water flux across composite membranes.

half that of the CA80 membrane. The low apparent salt diffusion coefficient may, therefore, represent the combined contributions of low porosity and high tortuosity in the BM-05 membrane.

Using the apparent diffusion coefficients shown in Table 2, the internal concentration polarization coefficient, Q, can be calculated as a function of water flux. The resulting curves for the membranes studied are shown in Figure 16. Since internal concentration polarization and the water flux through the membrane are directly proportional, this figure shows the maximum flux obtainable, regardless of further osmotic pressure increases. Clearly, only the CA80 and PBIL membranes exhibit useful fluxes.

Although internal concentration polarization and, to a lesser extent, membrane compaction appear to be the dominant effects in PRO, osmotic deswelling can also be detected. For example, Figure 17 shows the osmotic flux calculated from the apparent salt diffusion coefficient, D_a, plotted vs. brine concentration. When this calculated curve is compared with the experimental data, there is a marked disagreement at high brine concentrations. This effect is consistent with osmotic deswelling of the membrane with concentrated salt solutions, in this case above approximately 10% w/v NaCl.

B. Salinity Gradient Systems: Sodium Chloride Brines/Seawater, Sodium Chloride Brines/Brackish Water

In regions where concentrated sodium chloride brines are found, fresh water supplies are frequently very limited and the use of brackish water may be more practicable. Using NaCl brines on the concentrated side and seawater or brackish waters on the dilute side of the membrane is therefore an alternative method of increasing the potential utility of the salinity gradient resource found in salt lakes. Experiments aimed at determining the effect on osmotic flux of the salt concentration on the dilute side of the membrane were performed using PBIL and PA-300 membranes. These membranes were chosen to represent the asymmetric and composite types of membranes, respectively. The high concentration side of the membrane was maintained at 25% w/v NaCl, and the dilute side salt concentration was varied. The results are shown in Figures 18 and 19 for PBIL and PA-300, respectively. The flux through each membrane decreased drastically with increasing salt concentration on the dilute side, in agreement with the prediction of rapidly increasing internal concentration polarization with increasing C_4/C_2 ratio, as illustrated in Figure 7.

TABLE 2. Comparison of experimental direct osmosis water fluxes from sodium chloride brines to the values predicted from reverse osmosis data.

Membrane	Water Flux with (3.5% w/v NaCl (gfd) Extrapolated from Direct Osmosis Data	Projected from Reverse Osmosis Experiments	Ratio of Direct Osmosis Water Flux to Reverse Osmosis Water Flux	Apparent Diffusion Coefficient in the Sublayer, D_a (cm^2/sec)
Composite Membranes				
PA-300	0.60	6.49	0.09	3.5×10^{-7}
NS-101	0.08	5.93	0.01	$\sim 1.5 \times 10^{-8}$
NS-200	1.70	5.93	0.29*	3.3×10^{-7}
BM-1-C	0.60	3.50	0.20	3.0×10^{-7}
Low-Rejection Asymmetric Membranes				
CA70	5.40	9.93	0.54	2.5×10^{-5}
High-Rejection Asymmetric Membranes				
CA80	9.20	5.26	1.80	$\sim 1.5 \times 10^{-5}$
BM-05	1.20	2.42	0.50	5.7×10^{-7}
PBIL	6.00	3.36	1.80	3.5×10^{-6}

* Simultaneous and continuous increases in water and salt fluxes were noted in the direct osmosis experiments with the NS-200 membrane, suggesting some membrane instability.

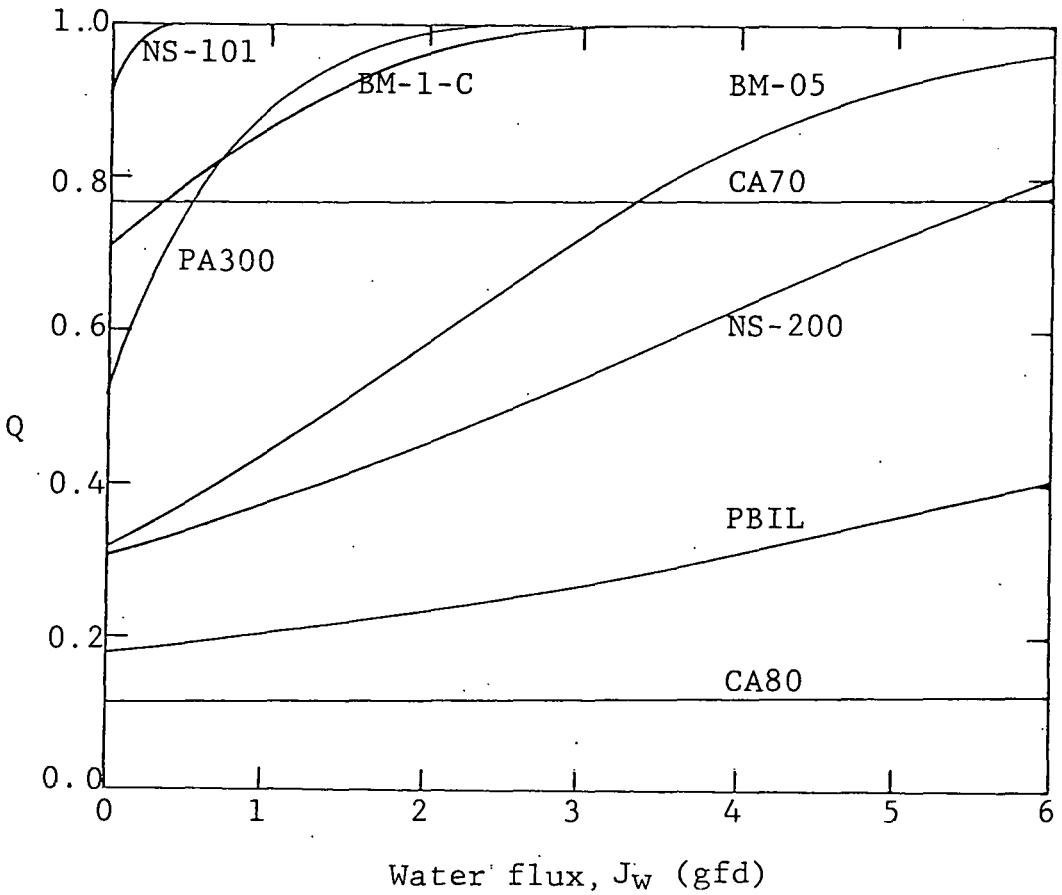

Figure 16. Calculated internal concentration polarization coefficient, Q, vs. steady state direct osmosis water flux. The calculation is based upon the apparent diffusion coefficient, D_a, of sodium chloride in the porous sublayer of each membrane.

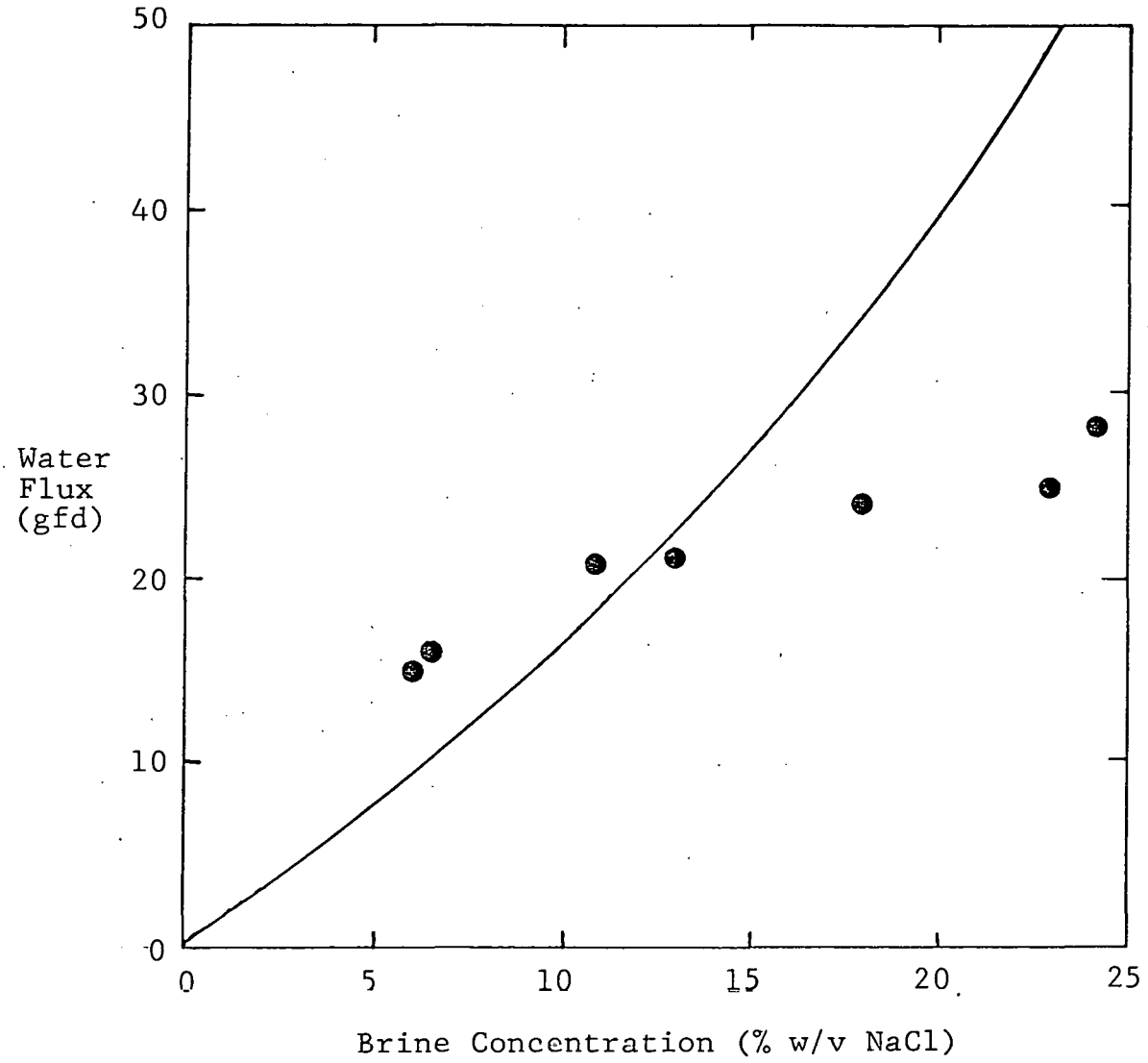

Figure 17. Comparison between direct osmosis data of CA80 and the predicted water flux based upon an effective diffusion coefficient of 1 x 10^{-5} cm^2/sec.

[● Data; —— Equation 11]

internal concentration polarization model presented earlier, and knowing the observed and expected value of the flux and the membrane thickness, an apparent diffusion coefficient in the substructure can be calculated which would satisfy the data in Table 2. In the absence of detailed structural information about the membranes listed, it is difficult to estimate the relative effects of τ, ε, and D_s on salt diffusion. It is therefore convenient to define the apparent diffusion coefficient as follows:

$$D_a \equiv \frac{D_s \varepsilon}{\tau} \qquad (14)$$

Using the experimental data and Equation (14), the values of D_a have been calculated for all of the membranes listed in Table 2. The values for the composite membranes are on the order of 1×10^{-7} to 1×10^{-8} cm^2/sec, significantly lower than those observed in the asymmetric membranes.

The CA70 membrane represents the second type of membranes, namely low-rejection Loeb-Sourirajan-type membranes. The CA50 and CA60 membranes also belong to this group, but their salt rejections were so low that they were not further tested experimentally. The CA70 membrane also suffers from severe internal concentration polarization, in this case caused by the high flux of salt through the rejecting skin layer of this membrane. The apparent diffusion coefficient for CA70 is 2.5×10^{-5} cm^2/sec, practically equal to the free solution diffusivity of sodium chloride in water, as would be expected from the highly porous structure of these membranes. However, even at this high diffusion coefficient, the salt cannot be removed fast enough from the membrane substructure to avoid concentration polarization and a consequent reduced osmotic flux.

The final class of membranes are the high-rejection asymmetric (Loeb-Sourirajan) membranes. These membranes appear to fall into two sub-groups. The first group includes the CA80 and PBIL membranes, which have even higher fluxes than predicted from RO conditions. This effect is likely caused by compaction of the porous membranes under the high hydrostatic pressures of reverse osmosis. The open, porous structure of these membranes is verified by the high apparent salt diffusion coefficient of 1.5×10^{-5} cm^2/sec.

The results for the second type of asymmetric membranes, polyamide BM-05, are rather anomalous. Based on the observed osmotic fluxes, the apparent salt diffusion coefficient is 5.7×10^{-7} cm^2/sec, definitely a low value for an asymmetric membrane. On the other hand, this does appear to be a rather dense membrane, with a water permeability less than

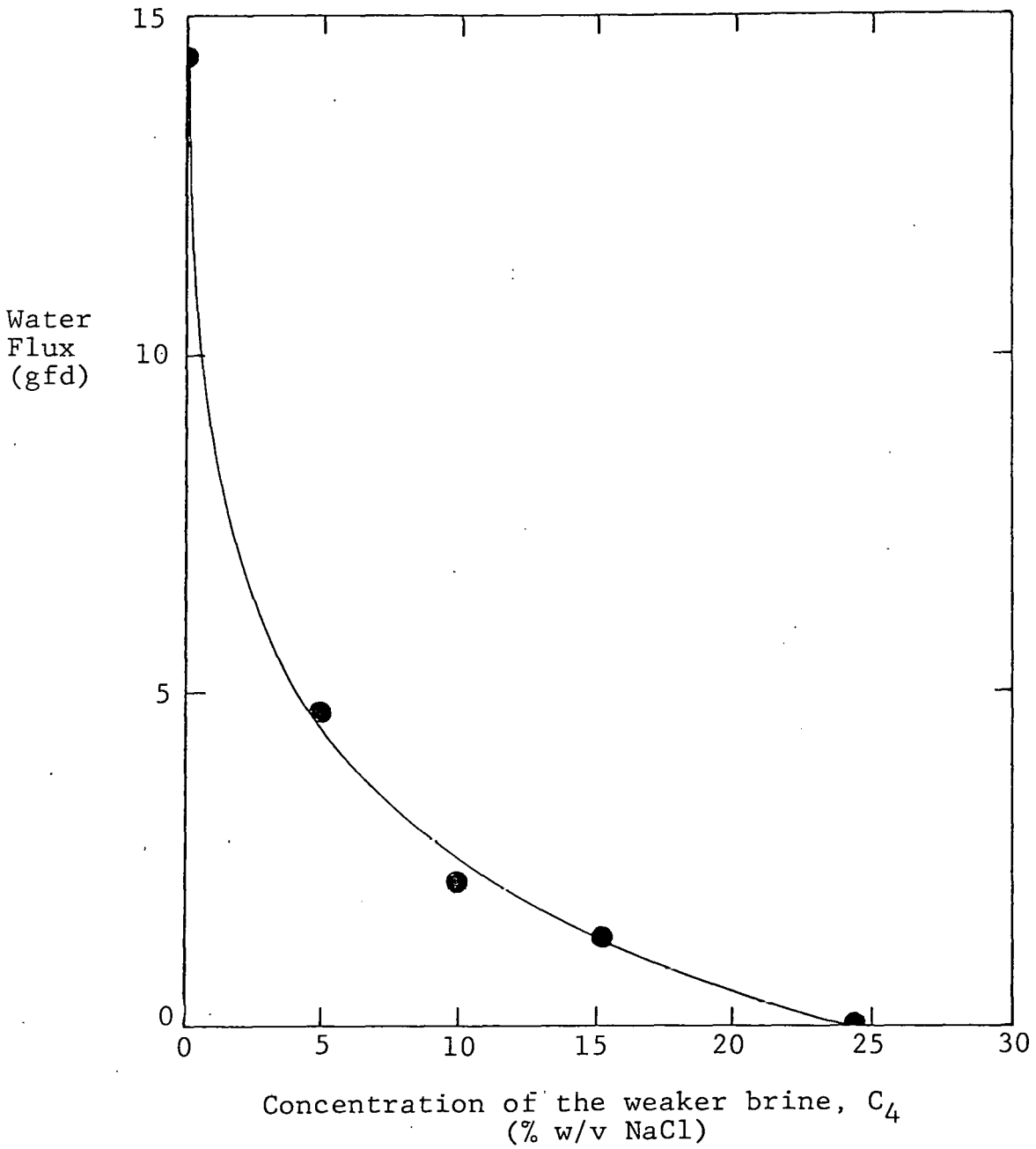

Figure 18. Effect of the dilute side salt concentration on the direct osmosis water flux through a PBIL membrane.

[● Experimental data; —— Equation (10) with $D_a = 3.5 \times 10^{-6}$ cm^2/sec.]

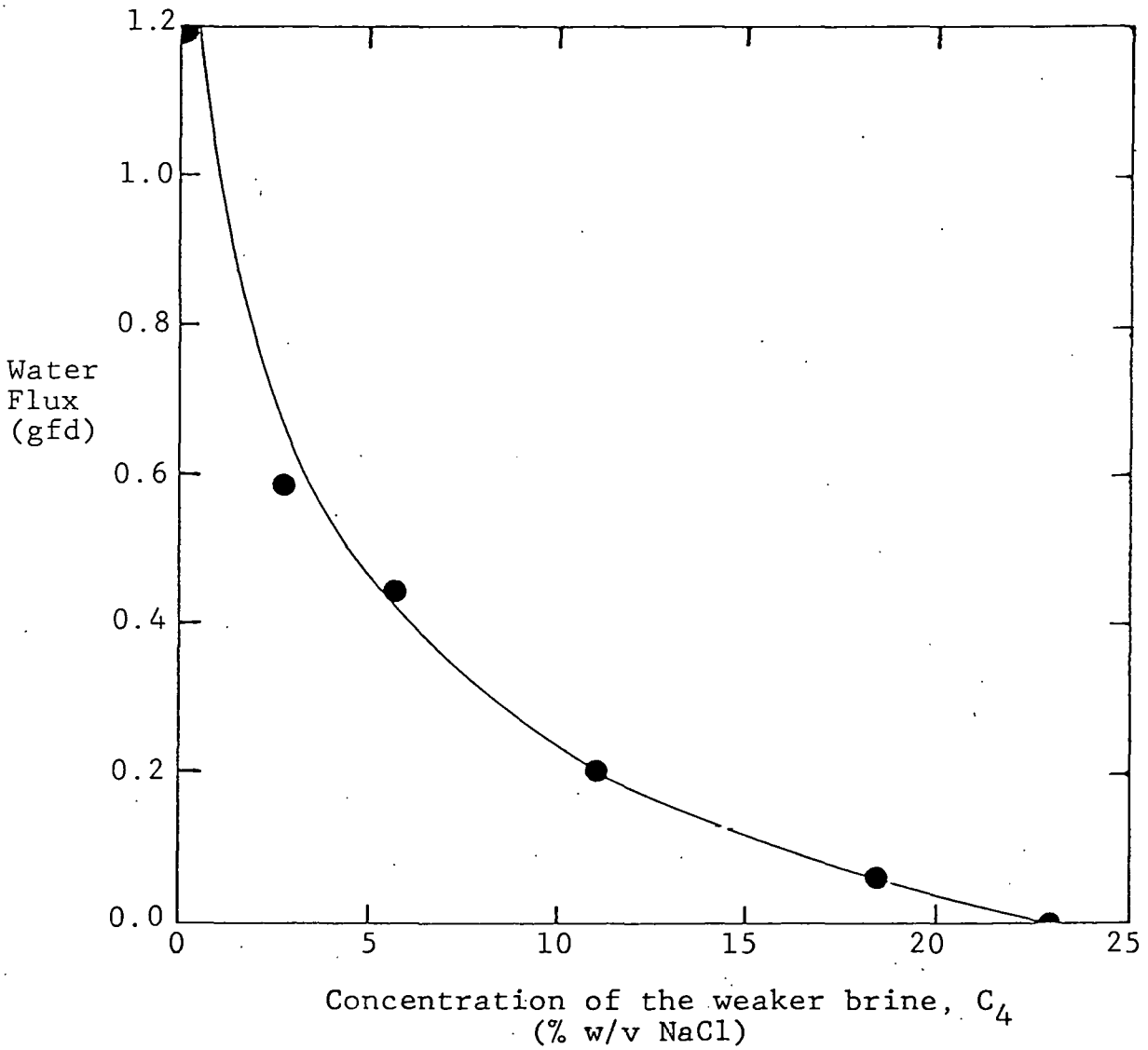

Figure 19. Effect of the dilute side salt concentration on the direct osmosis water flux through a PA-300 membrane.

[•Experimental data; —— Equation (10) with $D_a = 3.5 \times 10^{-7}$ cm^2/sec]

If internal concentration polarization characteristics can be adequately modelled by a single value of the apparent diffusion coefficient, then Equation (10) may be employed to regenerate the water flux vs. NaCl concentration data. The solid curves in Figures 18 and 19 represent the theoretical dependence of the water flux on the NaCl concentration on the dilute side, using D_a values of 3.5×10^{-6} cm^2/sec and 3.5×10^{-7} cm^2/sec for PBIL and PA-300, respectively. Excellent agreement is obtained.

The internal concentration polarization behavior of the two membranes can further be illustrated by constructing Q vs. J_w families of curves calculated from Equation (10) for different salt concentration ratios (C_4/C_2). These plots are shown in Figures 20 and 21, along with the actual flux data from Figures 18 and 19. The fit of the experimental flux data reveals that for each membrane, there may exist a unique value of the internal concentration polarization parameter, Q, for all C_4/C_2 ratios. It is thus possible to predict the DO flux at any C_4/C_2 ratio using the Q value determined from a single experiment. For these two membranes, the value of Q is about 0.8 for PBIL and 0.9 for PA-300. The relatively high values for both membranes suggest that DO systems would operate at fairly high internal concentration polarization under a wide variety of boundary conditions and membrane structural characteristics.

From Figures 18 and 19, the water flux through each membrane at 3.5% NaCl (the concentration of salt in seawater) was approximately half of the value when fresh water was used. It appears, therefore, that the system, NaCl brines/Seawater, is not a viable salinity gradient resource. Brackish waters could be used, provided their concentrations do not exceed approximately 1% NaCl.

C. Salinity Gradient System: Magnesium Sulfate Brines/Water

One possible method of overcoming the internal concentration polarization problem that occurs with sodium chloride brines is to use a more highly rejected salt, such as magnesium sulfate. A series of experiments with $MgSO_4$ brines was therefore performed, using essentially the same procedure as that employed with the NaCl brines. The membranes were first characterized by reverse osmosis experiments, after which the direct osmosis flux at various $MgSO_4$ concentrations was measured. The effects of internal concentration polarization, compaction, and osmotic deswelling were then obtained by comparing the RO and DO results.

The RO flux and rejection data are shown in Table 3. Magnesium sulfate was rejected significantly better than NaCl: all of the membranes had rejections between 97% and 100% except CA70, where the rejection remained relatively low at 45%.

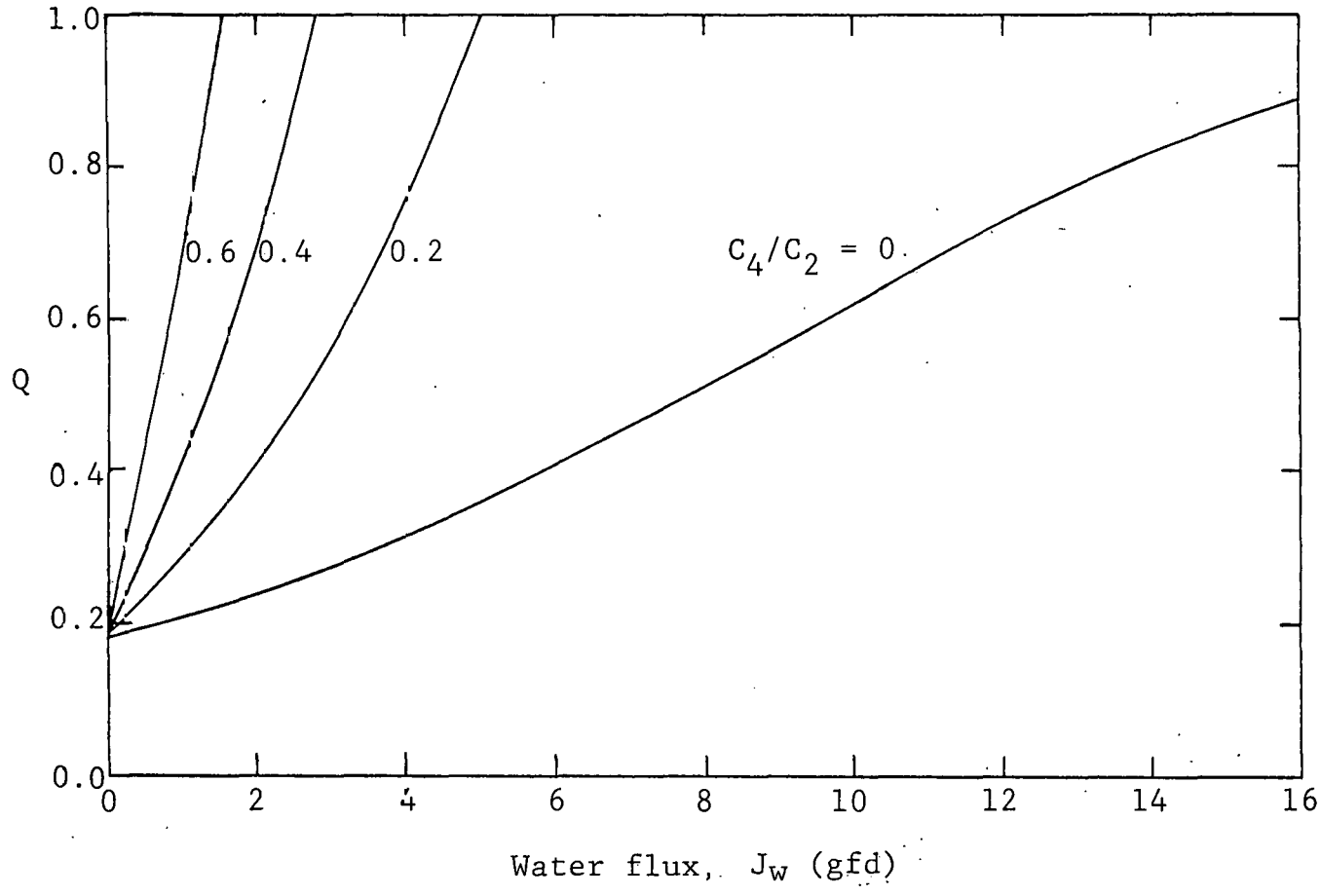

Figure 20. Internal concentration polarization characteristics of a PBIL membrane at different brine concentration ratios of sodium chloride.

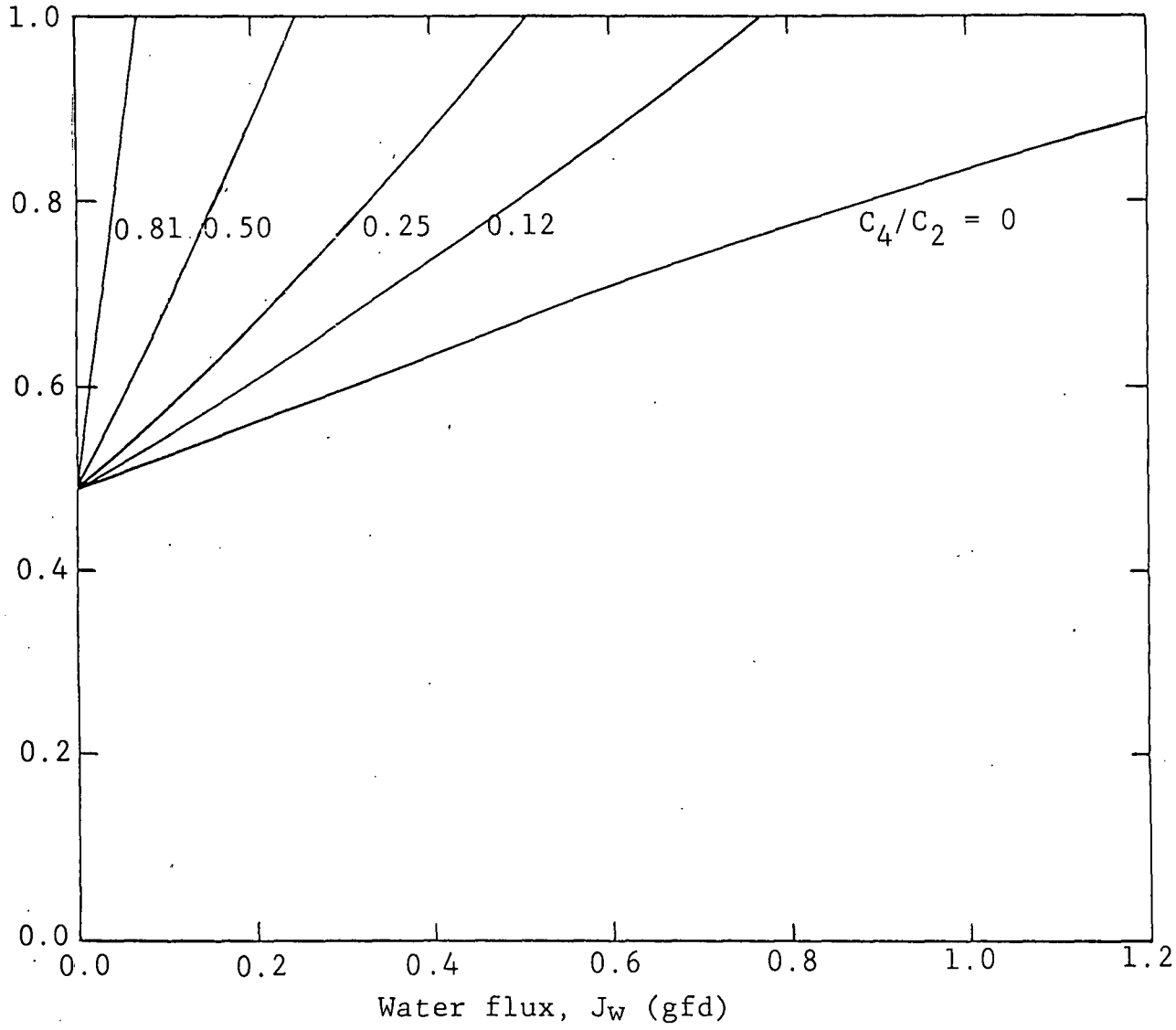

Figure 21. Internal concentration polarization characteristics of a PA-300 membrane at different brine concentration ratics of sodium chloride.

TABLE 3. Transport properties of several RO membranes and their projected direct osmosis performance with 1% w/v magnesium sulfate, $\Delta\pi$ = 2.72 atm.

Membrane	Membrane Thickness (cm)	Water Permeation Constant, A ($\frac{cm^3}{cm^2\text{-sec-atm}}$)	Salt Rejection (%)	Salt Permeation Constant, B (cm/sec)	Observed Osmotic Pressure $\Delta\pi_{obs}$ (atm)	Theoretical Maximum Direct Osmosis Water Flux ($\frac{cm^3}{cm^2\text{-sec}}$)	Theoretical Maximum Direct Osmosis Water Flux (gfd)	Theoretical Maximum Available Work (watt/ft^2)
Cellulose Acetates								
CA80	9.65×10^{-3}	1.9×10^{-5}	97.9	3.3×10^{-5}	2.7	5.0×10^{-5}	1.10	3.2×10^{-3}
CA70	9.40×10^{-3}	2.4×10^{-5}	45.0	2.3×10^{-3}	1.2	2.9×10^{-5}	0.62	8.4×10^{-4}
Polyamide								
BM-05	1.14×10^{-2}	6.3×10^{-6}	99.97	1.5×10^{-7}	2.7	1.7×10^{-5}	0.36	1.1×10^{-3}
Polybenzimidazolone								
PBIL	2.4×10^{-2}	7.0×10^{-6}	97.9	1.2×10^{-5}	2.7	1.9×10^{-5}	0.40	1.2×10^{-3}
Composites								
PA-300	2.03×10^{-2}	1.7×10^{-5}	99.92	1.1×10^{-6}	2.7	4.7×10^{-5}	0.99	3.0×10^{-3}
NS-101	4.32×10^{-3}	1.6×10^{-5}	99.48	6.7×10^{-6}	2.7	4.4×10^{-5}	0.94	2.8×10^{-3}
NS-200	4.06×10^{-3}	6.5×10^{-6}	98.4	8.4×10^{-6}	2.7	1.8×10^{-5}	0.37	1.1×10^{-3}
BM-1-C	1.17×10^{-2}	1.1×10^{-5}	97.9	1.8×10^{-5}	2.7	2.8×10^{-5}	0.59	1.8×10^{-3}

The results of the direct osmosis experiments are shown in Figures 22 and 23 for the asymmetric and composite membranes, respectively. As with NaCl brines, the fluxes for most of the membranes were significantly lower than the fluxes expected from the RO data. The DO and RO data are compared in Table 4, which also includes the apparent salt diffusion coefficient (D_a) for $MgSO_4$, calculated using the internal concentration polarization model and Equation (14).

The composite membrane DO fluxes are all significantly lower than the flux predicted from RO. The apparent salt diffusion coefficients range from 1×10^{-9} to 1×10^{-7} cm^2/sec. Although less $MgSO_4$ permeates the membrane skin, the diffusion coefficient in the underlying substructure is lower as well, resulting in even worse internal concentration polarization with $MgSO_4$ than with NaCl for the composite membranes. This behavior is illustrated by plotting the internal concentration polarization coefficient, Q, against membrane flux, as shown in Figure 24. The CA70 membrane, representative of the low-rejecting asymmetric membranes, had a higher flux in DO experiments than expected from the extrapolated RO results. This is the reverse of the case when NaCl was used instead of $MgSO_4$. The slightly lower $MgSO_4$ leakage through the membrane reduced the internal concentration polarization in the DO experiments, resulting in a relatively small flux decrease. This flux decrease was more than offset by the flux increase due to the absence of the compaction present in the RO tests. Nonetheless, as was the case with the NaCl brines, CA80 and PBIL appear to be the most promising membranes for PRO.

D. Salinity Gradient System: Polyelectrolyte Brines/Water

An additional attempt to overcome the internal concentration polarization problem consisted of using polyelectrolyte brines on the salt (skin) side of the membrane. The rationale was that a polyelectrolyte, by being completely rejected by the membrane, would not suffer the flux reduction due to internal concentration polarization present with other brines. In addition, the presence of small counterions should create an appreciable osmotic pressure. The polyelectrolyte chosen was sodium polystyrene sulfonate (Polysciences Inc., Warrington, PA).

The DO results shown in Figure 25 for PBIL and PA-300 membranes (representative of asymmetric and composite membranes, respectively) were not encouraging. Even with very highly concentrated polyelectrolyte solutions, the osmotic fluxes were low. In fact, the DO flux through the PA-300 membrane, for unknown reasons, actually decreased with increasing polyelectrolyte concentration. Based on these results, polyelectrolyte salt brines do not appear to be a potentially useful PRO source.

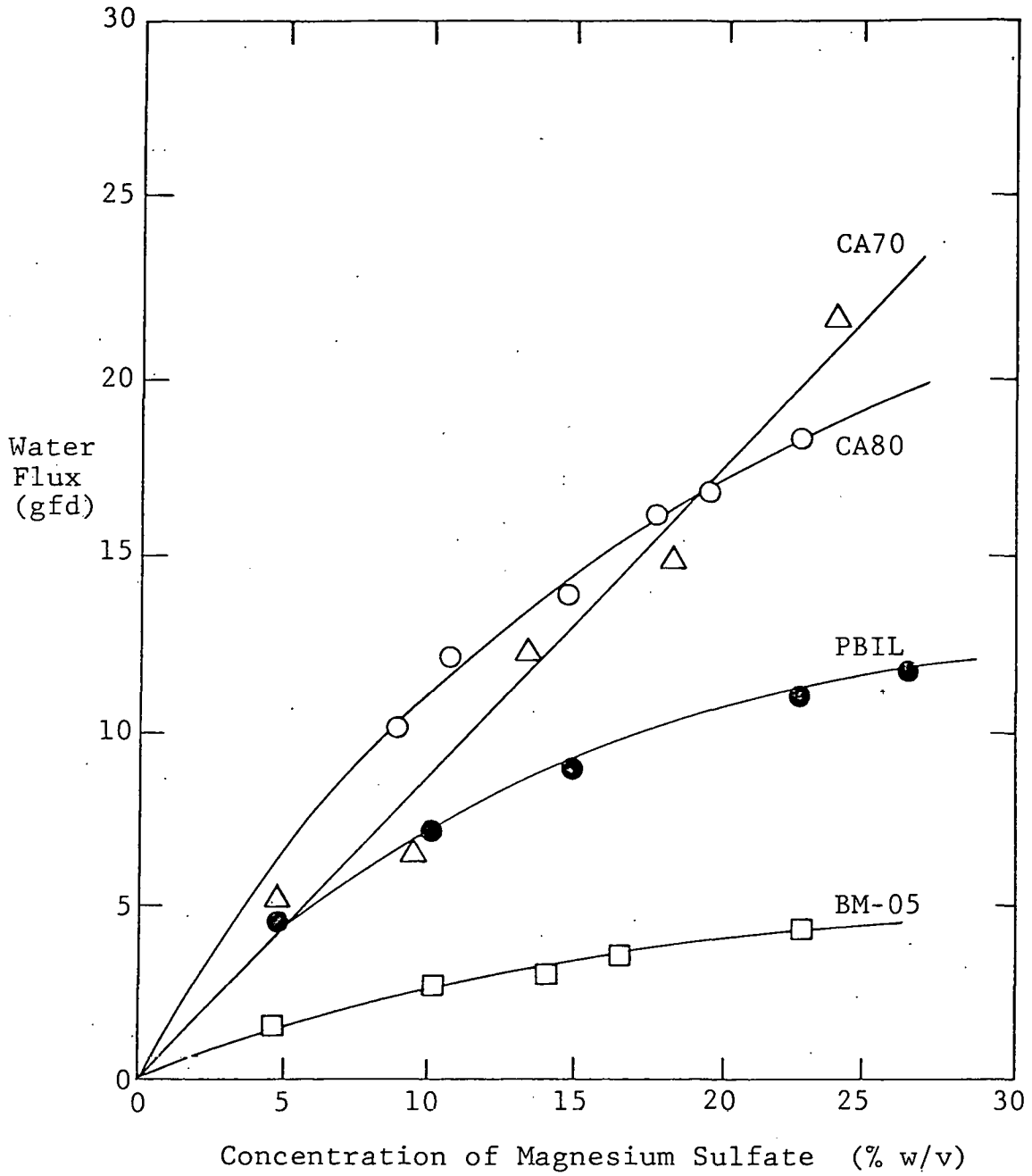

Figure 22. Effect of magnesium sulfate concentration on direct osmosis water flux across asymmetric membranes.

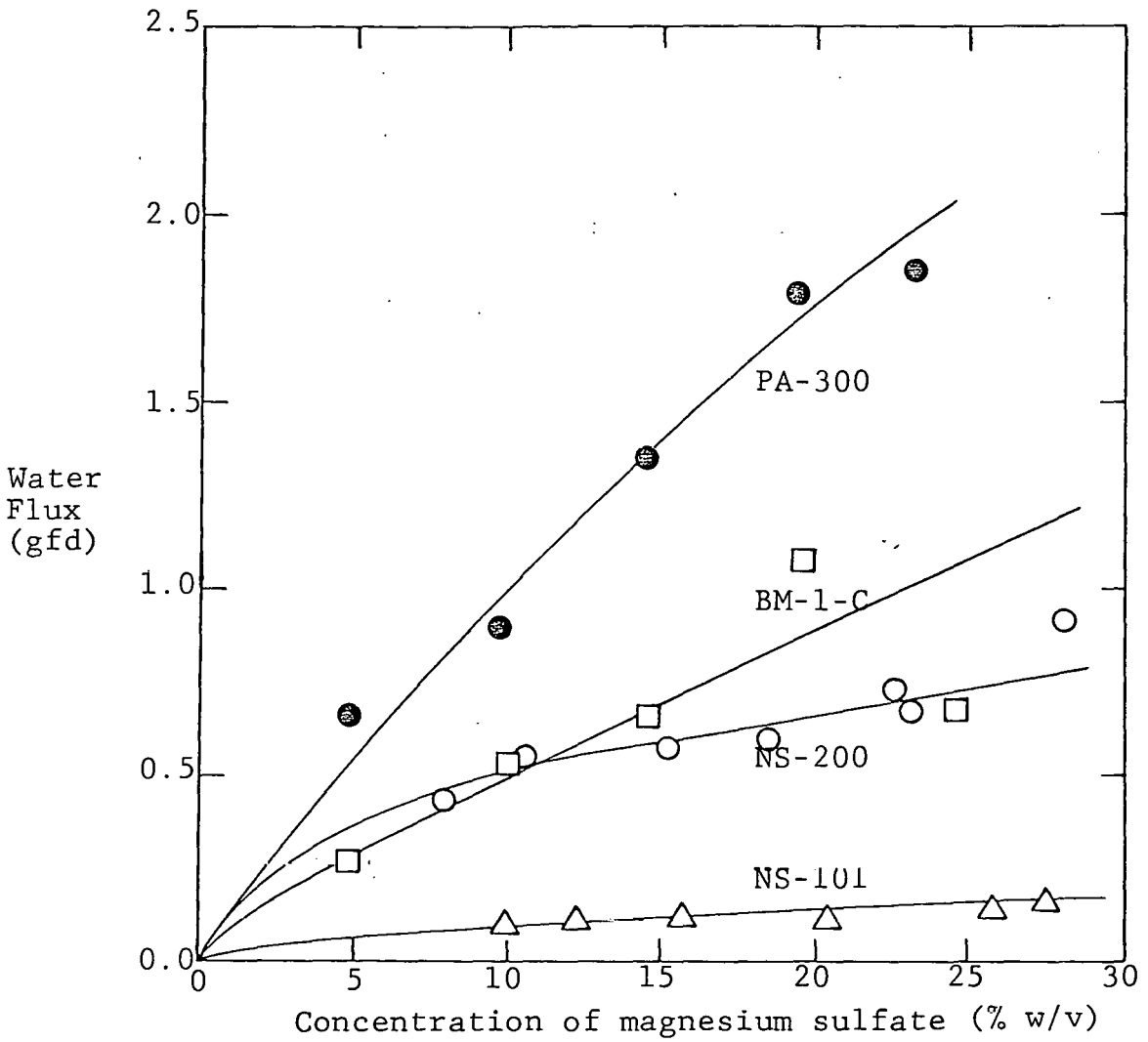

Figure 23. Effect of magnesium sulfate concentration on direct-osmosis water flux across composite membranes.

TABLE 4. Comparison of experimental direct osmosis water fluxes with magnesium sulfate brines to the values predicted from reverse osmosis data.

Membrane	Water Flux with 1% w/v $MgSO_4$(gfd)		Ratio of Direct Osmosis Water Flux to Reverse Osmosis Water Flux	Apparent Diffusion Coefficient in the Sublayer, D_a(cm^2/sec)
	Extrapolated from Direct Osmosis Data	Projected from Reverse Osmosis Experiments		
Composite Membranes				
PA-300	0.14	0.99	0.14	2.0×10^{-7}
NS-101	0.01	0.94	0.02	5.0×10^{-9}
NS-200	0.08	0.37	0.22	3.3×10^{-8}
BM-1-C	0.08	0.59	0.14	1.1×10^{-7}
Low-Rejection Asymmetric Membranes				
CA70	1.10	0.62	1.80	5.0×10^{-5}
High-Rejection Asymmetric Membranes				
CA80	1.80	1.07	1.70	$\sim 1.0 \times 10^{-5}$
BM-05	0.33	0.36	0.92	2.7×10^{-7}
PBIL	1.10	0.40	2.80	$\sim 5.0 \times 10^{-5}$

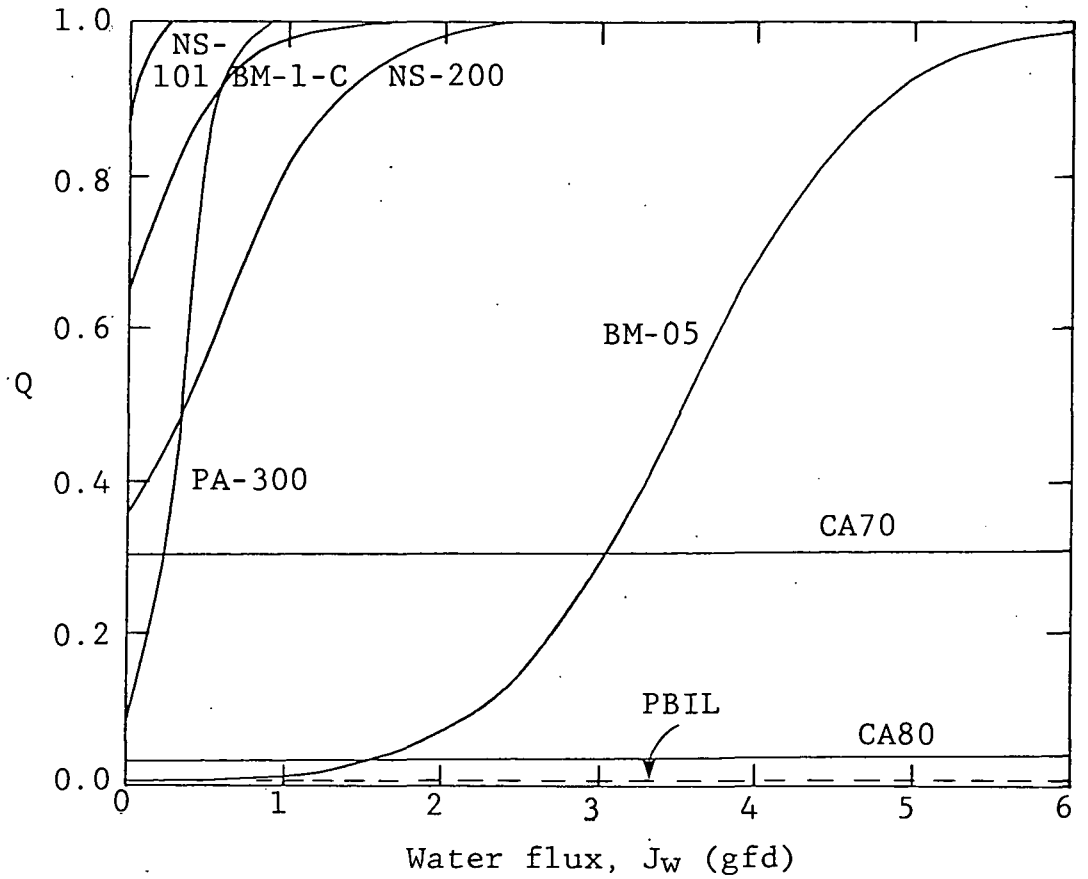

Figure 24. Calculated internal concentration polarization coefficient, Q, vs. steady state direct osmosis water flux. The calculation is based on the apparent diffusion coefficient, D_a, of magnesium sulfate in the porous sublayer of each membrane.

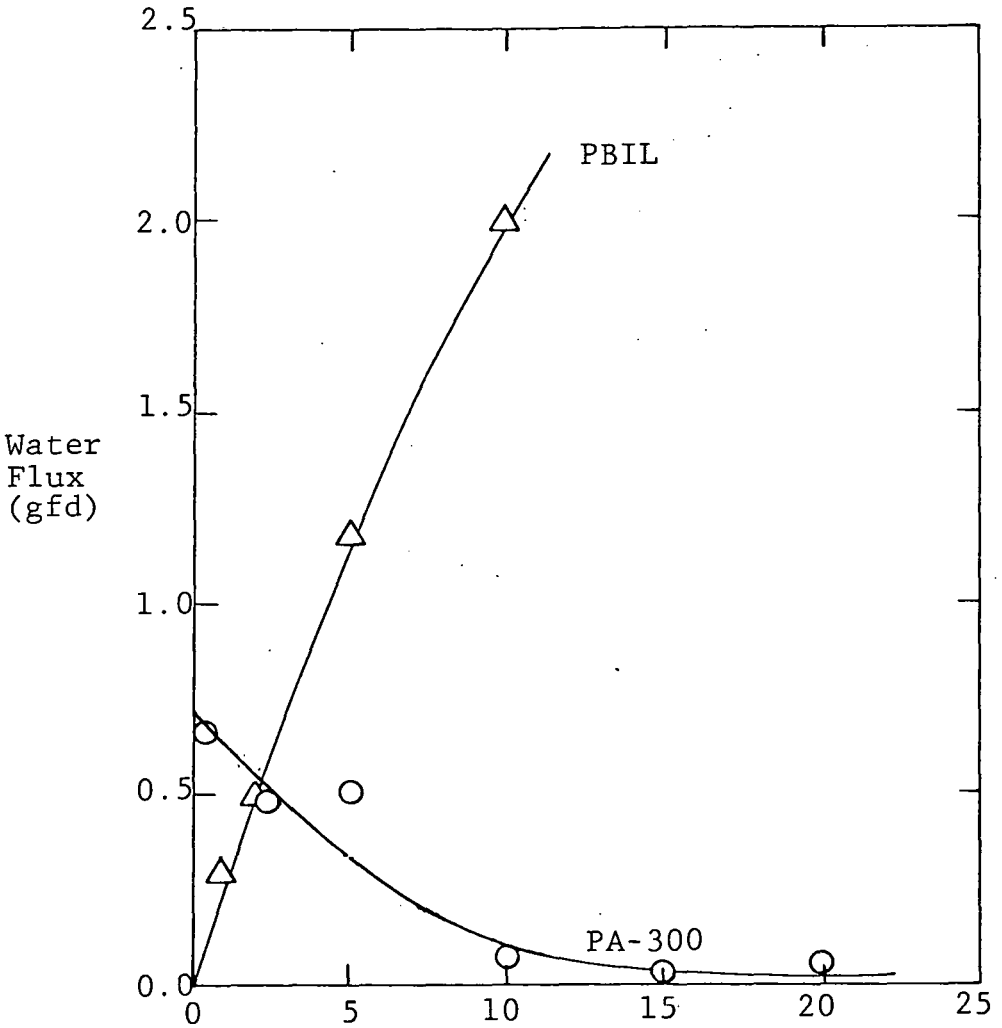

Figure 25. Effects of polyelctrolyte concentration on direct osmosis water flux.

V. ECONOMICS OF PRO POWER GENERATION

The operating costs of a PRO power plant are likely to be relatively low, since the processes use a renewable resource. Capital costs, however, are likely to be high, so for simplicity, only the capital costs will be considered in the first crude analysis of process economics. For further simplicity, it is also assumed that the system operates at the maximum power generating capacity per unit membrane area, in which case the power production is given by Equation (2):

$$\text{power/unit membrane area} = \frac{A\Delta\pi^2}{4}, \qquad (2)$$

where A is the membrane permeability constant and $\Delta\pi$ is the osmotic pressure difference across the membrane.

Based on the data shown in this report, the CA80 asymmetric membrane appears to be the most promising membrane. Thus, using the DO flux data from Figure 14 for the NaCl brines/water salinity gradient system, together with Equation (2), it is possible to calculate the power per unit area of membrane. This data is shown in Figure 26 as a function of the NaCl concentration used. The dependence of power on the square of the osmotic pressure difference is easily seen. From this curve, the capital cost/kilowatt of power capacity follows directly from the cost/ft^2 of membrane area. Membrane costs range from approximately 30¢/ft^2 for hollow fiber RO membranes to \$2/ft^2 for flat sheet membranes.

Using the higher figure, Figure 26 shows that PRO is only marginally competitive with conventional power generators (a typical cost for conventional power generation is \$1000 per kilowatt capacity[18]), even if concentrated brines are used as the salinity gradient resource. On the other hand, if the hollow fiber cost of 30¢/ft^2 is used, the system is clearly competitive with conventional power generating methods using NaCl brines, and approaches conventional costs even if seawater is used as the salinity gradient resource. However, this favorable prognosis is valid only if the fluxes of flat sheet membranes can be obtained in a hollow fiber system. This would entail not only developing reliable hollow fiber membranes, but also minimizing internal concentration polarization effects. This cost analysis, as mentioned before, does not consider operating costs, which may become significant at the higher pressures of concentrated brines.

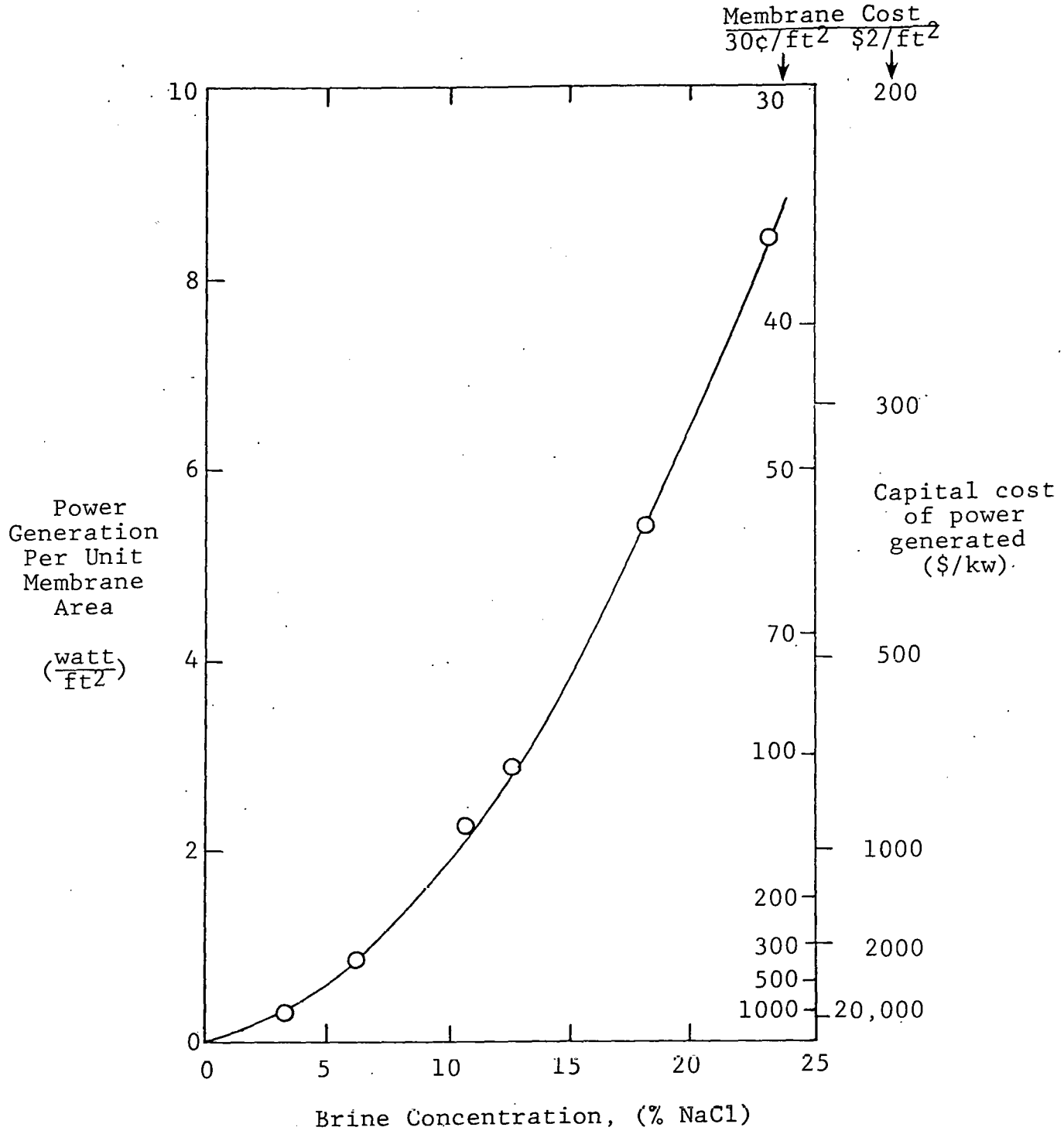

Figure 26. The maximum power per unit membrane area as a function of the sodium chloride concentration used in the brine. The membrane is the CA80 asymmetric membrane. Also shown is the capital cost of the power generated for two membrane costs.

VIII. REFERENCES

1. G.L. Wick and J.D. Isaacs, "Utilization of the Energy From Salinity Gradients", paper presented at the Workshop on Wave and Salinity Gradients Energy Conversion, University of Delaware (May, 1976).

2. S. Loeb, Journal of Membrane Science 1 (1976) 49.

3. H.H.G. Jellinek, "Osmotic Work I. Energy Production From Osmosis of Fresh Water/Saline Water Systems", paper presented at Workshop on Wave and Salinity Gradient Energy Conversion, University of Delaware (May, 1976).

4. S. Loeb, F. Van Hessen, and D. Shahaf, Journal of Membrane Science 1 (1976) 249.

5. G.L. Wick, Energy 3 (1978) 95.

6. H.K. Lonsdale, "Properties of Cellulose Acetate Membranes", in Desalination by Reverse Osmosis, U. Merten, (Ed.), The M.I.T. Press, Cambridge, MA (1966).

7. H.K. Lonsdale, U. Merten, and R.L. Riley, J. Appl. Polym. Sci. 9 (1965) 1341.

8. R.A. Robinson and R.H. Stokes, Electrolyte Solutions, 2nd Ed., Butterworths, London (1959) 513-515.

9. F.K. Lesan, et al. OSW Research and Development Progress Report No. 879, Dept. of the Interior, Washington, D.C., (September, 1973).

10. G.L. Wick and J.D. Issacs, Science 199 (1978) 1436.

11. S. Manjikian, S. Loeb, and J.W. McCutchan, Proc. First International Symposium on Water Desalination, Washington, D.C., 1965; (published by U.S. Department of the Interior, Office of Saline Water, Washington, D.C.), Vol 2 (1965) 159-173.

12. H. Strathmann, H.D. Saier, and R.W. Baker, "The Formation Mechanisms of Asymmetric Reverse Osmosis Membranes", Proc. 4th International Symp. Fresh Water from the Sea, Heidelberg, W. Germany, (September, 1973); also, U.S. Patent 3,925,211 to W. Schumann and H. Strathmann.

13. S. Hara, K. Mori, Y. Taketani, T. Noma, and M. Seno, Desalination 21 (1977) 183-194.

14. R.L. Goldsmith, B.A. Wechsler, S. Hara, K. Mori, and Y. Taketani, Desalination 22 (1977) 311.

15. R.L. Riley, private communication.

16. R.J. Petersen and K.E. Cobian, American Electroplaters' Society Project 36, Plating and Surface Finishing (June, 1976) 51-57.

17. J.E. Cadotte, U.S. Patent 3,926,798 (December 16, 1975).

18. Hydroelectric Plant Construction Cost and Annual Production Expenses, Sixteenth Annual Supplement—1972, Federal Power Commission, Washington, D.C. (1975).

19. S. Sourirajan, Reverse Osmosis, Academic Press, New York, NY (1970), Appendix II.

Appendix

Osmotic Pressure of $MgSO_4$ and NaCl Solutions[19]

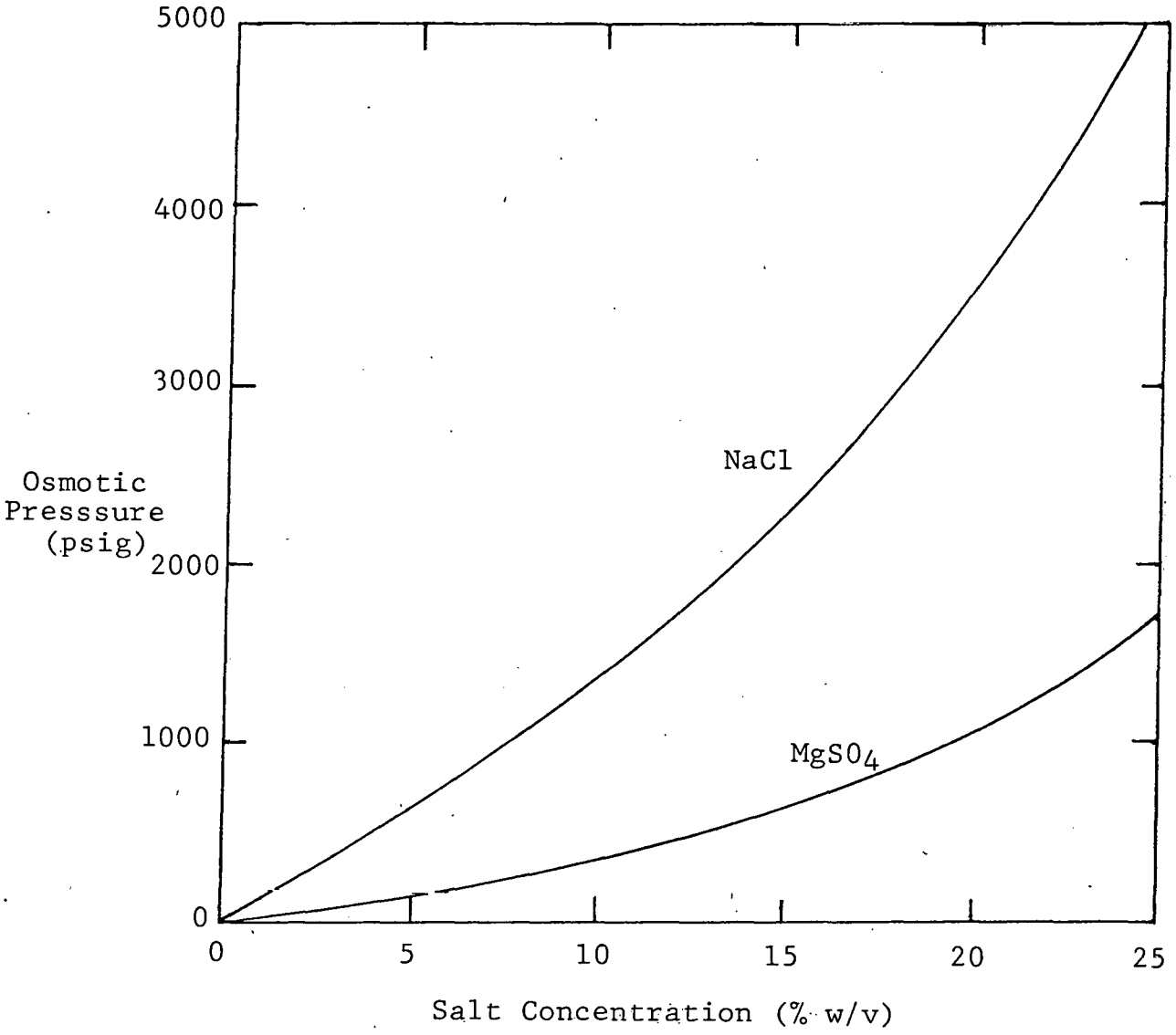
5000
4000
3000
2000
1000
0
Osmotic
Presssure
(psig)
NaCl
MgSO4
0
5
10
15
20
25
Salt Concentration (% w/v)